

12. CHRONOLOGY AND COMPOSITION OF VOLCANICLASTIC ASH LAYERS IN THE CENTRAL TYRRHENIAN BASIN (SITE 974)¹

Paul van den Bogaard,² Beate Mocek,² and Marianne Stavesand²

ABSTRACT

Petrographic descriptions, major-element glass compositions, and laser $^{40}\text{Ar}/^{39}\text{Ar}$ ages are presented for Pliocene–Pleistocene tephra layers and volcaniclastic sediments of cores from Hole 974B, drilled during Ocean Drilling Program Leg 161. Individual fallout ash layers and volcaniclastic turbidites show highly diagnostic glass particle morphologies and a wide spectrum of silicic to intermediate major-element compositions, ranging from low-K calc-alkaline, to high-K calc-alkaline, high-K shoshonitic, and to alkaline magma suites. High-K shoshonitic components and individual ash layers are derived mainly from explosive eruptions on Ponza (Pontian Islands) between 3 Ma and 0.8 Ma. Single-crystal and step-heating $^{40}\text{Ar}/^{39}\text{Ar}$ analyses of tephra layers from 33.07 meters below seafloor (mbsf) (Sample 161-974B-4H-6, 6–7 cm) and 28.33 mbsf (4H-2, 132–134 cm) yield eruption ages of 0.51 ± 0.02 and 0.42 ± 0.04 Ma, respectively. Step-heating analyses of biotite crystals from volcaniclastic crystal-lithic sands yield ages from 74 to 291 Ma, which indicate a detrital origin from pre-alpine granitoids (Sardinia?). Six tephrostratigraphic markers are defined on the basis of glass shard compositions and morphologies.

INTRODUCTION

Tephra fallout layers and volcaniclastic sediments, derived from volcanic sources around and within the Tyrrhenian Sea, form an important component of the detrital sediments deposited in the Tyrrhenian backarc basin. The tephra layers and volcaniclastic material also provide chronostratigraphic markers in the sedimentary sequences and record the earlier temporal and compositional evolution of the volcano-magma systems involved, which are often eroded on land or hidden by accumulations of younger tephra and lava.

The Tyrrhenian magmatic provinces and volcanic eruptive centers were highly productive during most of the Pliocene–Pleistocene until the present. Up to 151 different primary tephra deposits derived from explosive eruptions in the Campanian province, the active arc of the Eolian Islands, from Pantelleria and Etna, were identified in cores spanning the last 190,000 yr (Keller et al., 1978; Paterne et al., 1990). The earlier, Pliocene–Pleistocene, volcanic evolution and tephrostratigraphy was studied in the eastern Mediterranean during Ocean Drilling Program (ODP) Leg 107, but remained incomplete, because of rotary drilling limitations and discontinuous recovery of stratigraphic sequences older than ~130,000 yr (McCoy and Cornell, 1990; Calanchi et al., 1994).

During ODP Leg 161, three advanced piston coring system (APC) and extended coring system (XCB) holes were drilled in the western Tyrrhenian Basin (Site 974) (Fig. 1). Site 974 is located on the lower eastern slope of the Sardinian continental margin, ~215 km east of Sardinia, on the western side of De Marchi Seamount (Fig. 1; Table 1). The principal objective of drilling at Site 974 was to retrieve a Pliocene–Pleistocene sedimentary sequence and a comprehensive record of organic-rich sapropel layers and volcaniclastic deposits. In this paper, we report the initial results of geochemical investigations and age determinations of volcaniclastic deposits from Hole 974B. Our objectives are (1) to characterize the petrographic and chemical composition of volcanic and volcaniclastic deposits from Hole 974B; (2) to correlate individual deposits to compositionally equivalent terrestrial source areas (i.e., Aeolian Arc, Campanian and Roman Vol-

canic Provinces) and tephrostratigraphic markers established during previous drilling in the Tyrrhenian Basin (Deep Sea Drilling Project Hole 373, ODP Leg 107, KET; Paterne et al., 1990); and (3) to contribute to a more comprehensive framework of the temporal and compositional evolution of explosive volcanism in the Tyrrhenian backarc system.

SAMPLES AND LABORATORY PROCEDURES

Ash-bearing layers totalling 207 were visually identified from Hole 974B by the Shipboard Scientific Party (1996). The layers consist of 111 ash-bearing horizons only a few millimeters thick, and 96 ash beds with thicknesses in the centimeter to decimeter range. The most prominent volcaniclastic deposits, with thicknesses >1 m, were obtained from the Pleistocene sequence at 12.5 meters below seafloor (mbsf) (Sample 161-974B-2H-4, 0–150 cm), and from the top of the Pliocene sequence at 80.83 mbsf (Sample 161-974B-9H-6, 33–145 cm). No ash-bearing layers were detected below Core 161-974B-15H at 131.45 mbsf. For this study, 92 samples of ash-bearing horizons were kindly provided by the Leg 161 Shipboard Scientific Party.

All samples were wet sieved, and the grain-size fractions 63–125 μm and 125–250 μm were mounted on smear slides. Following microscopic inspection, 21 samples with significant (>5 vol%) contents of volcanic glass shards and crystals were selected for further study and were mounted in polished thin sections (Table 2).

Major-element compositions of fresh glass shards were determined using a CAMECA SX 50 electron microprobe (EMS), operated at an accelerating voltage of 15 kV and a beam current of 10 nA. To minimize sodium loss, sodium was analyzed on rhyolitic glass shards using a beam size of $12 \times 11 \mu\text{m}$. Basaltic and intermediate glass shards were analyzed using a beam size <10 μm . Each element was determined by measuring for 20 s at the peak position and for 10 s at the background position. International and internal glass standards measured for comparison included the obsidian standards LIPARI (Cannetto Lami lava, Lipari; Hunt and Hill, 1993) and KN18 (Nielsen and Sigurdsson, 1981), and the basalt standards ALV 981 (submarine basalt; N. Metrich, pers. comm., 1995), and JdF-D2 (MORB basalt; C. Langmuir, pers. comm., 1995) (Table 3).

Standard deviations range from 0.01 to 0.60 wt%, with SiO_2 showing the highest standard deviation values and the highest concentrations. The recovery (measured concentration/standard concen-

¹Zahn, R., Comas, M.C., and Klaus, A. (Eds.), 1999. *Proc. ODP, Sci. Results*, 161: College Station, TX (Ocean Drilling Program).

²GEOMAR Forschungszentrum, Wischhofstrasse 1-3, D-24148 Kiel, Federal Republic of Germany. pbogaard@geomar.de

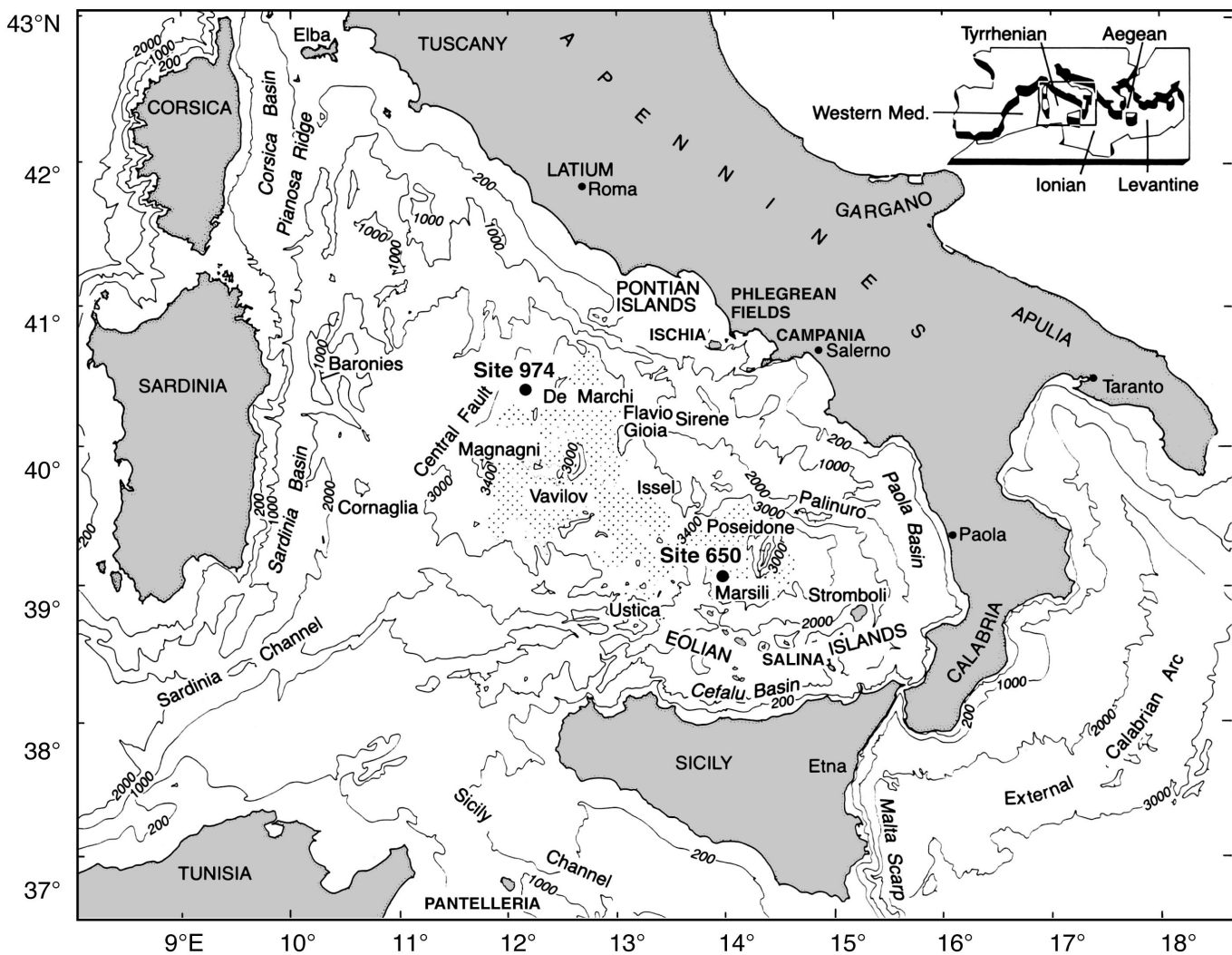


Figure 1. Location and setting of Site 974 in the central Tyrrhenian Sea. Location of Site 650, Leg 107, for comparison. Modified from Kastens, Mascle, Auroux, et al. (1987).

Table 1. Statistics for Hole 974B.

Site 974	
Latitude:	40°21.362'N
Longitude:	12°8.516'W
Water depth (m):	3453.9
Total penetration (m):	203.7
Total length of cored section (m):	203.7
Core recovery (%):	102.2
Oldest sediment cored:	
Depth (mbsf):	203.7
Earliest age:	Miocene

Note: Data from Comas, Zahn, Klaus, et al. (1996).

tration $\times 100$) of the standard analyses is generally within 95%–105% of the published standard values, but is significantly higher for MnO and P₂O₅ and lower for F and Cl analyses of rhyolite standards. Because rhyolite glass shards can exhibit H₂O contents up to 7 wt% (Bitschene and Schmincke, 1990), but undergo increasing loss of alkalies (i.e., sodium) during progressive hydration and alteration, only rhyolite glass shard analyses with totals >90–91 wt% were accepted (Froggatt, 1992). Glass particle size permitting, individual glass shards were analyzed repeatedly at different spots. Thus, up to four measurements were obtained per glass shard. Average major-element compositions are compiled in Table 4.

Age determinations by laser ⁴⁰Ar/³⁹Ar analysis were performed on sanidine and biotite crystals that were handpicked from selected samples, etched in dilute hydrofluoric acid (sanidine only), and cleaned using an ultrasonic disintegrator (both). Sanidines were analyzed by single-crystal total fusion. Biotite analyses were performed by laser step-heating to obtain gas samples with reduced levels of atmospheric argon contamination, following preferential degassing of atmospheric argon during low-temperature heating steps. Analyses of ⁴⁰Ar/³⁹Ar were performed at the Geomar Tephrochronology Laboratory, using a 25-W Spectra Physics argon ion laser and a MAP 216 series mass spectrometer. Raw mass spectrometer peaks were corrected for mass discrimination, background and blank values (determined every five analyses), and interfering neutron reactions on Ca and K using CaF₂ and K₂SO₄ salt crystals that were irradiated together with the samples. Correction factors were determined as ³⁶Ar/³⁹Ar_{Ca} = 0.465 ± 0.001, ³⁷Ar/³⁹Ar_{Ca} = 977 ± 2, ³⁸Ar/³⁹Ar_K = 0.0222 ± 0.0001, and ⁴⁰Ar/³⁹Ar_K = 0.002 ± 0.001. Irradiations were performed in the 5-MW research reactor of the GKSS Research Center (Geesthacht, Federal Republic of Germany) with crystals in aluminum trays and irradiation cans wrapped in 0.7-mm Cd foil. The neutron flux was monitored using TCR sanidine (Taylor Creek Rhyolite, 27.92 Ma; Dalrymple and Duffield, 1988; Duffield and Dalrymple, 1990) and an internal standard SAN6165 (469.8 Ka; Bogaard, 1995). Vertical variations in the neutron flux (J values) were quantified by a co-

Table 2. Tephra layers and volcaniclastic deposits, Hole 974B.

Core, section, interval (cm)	Depth (mbsf)	Sample no.	Sediment type	Thickness (cm)	Glass (%) [*]	Glass particle type	Crystals (%) [*]	Mineral assemblage	Lithics (%) [*]	Foraminifers (%) [*]	Zeolite (%)
1H-3, 57-58	3.54	7590	Volcaniclastic sand	12	10	Sp, id, md (<5%)	60	Kfsp, plag, qz, cpx, biot, tm	10	20	<1
1H-4, 17-18	4.68	7591	Volcaniclastic sand	2	40	Sb, sp, st	10	Kfsp, amph, biot	10	40	<1
1H-5, 28-29	6.29	7588	Volcaniclastic sand	<1	40	Sb, sp, st, md (<5%)	15	Kfsp, qz, biot, amph, cpx	15	30	<1
2H-1, 37-38	6.88	7601	Volcaniclastic turbidite	4	95	Sb, sd, id, md (<1%)	<1	Kfsp, amph, cpx	0	5	10
2H-3, 22-23	9.73	7600	Tephra	3	98	St, sp, id, md (<1%)	2	Kfsp, amph, plag, cpx, biot	<1	0	25
2H-4, 35-38	11.37	7513	Volcaniclastic sand	150	5	Sb, ib, id	75	Qz, kfsp, cpx, amph, plag	10	10	<1
2H-5, 63-64	13.14	7602	Volcaniclastic sand	4	40	Sb, sb, sd, st, ib, id	30	Kfsp, cpx, amph, tm, qz	0	30	5
2H-6, 42-43	14.43	7603	Volcaniclastic sand	3	<5	Sb, sd, st	70	Kfsp, cpx, sph, plag	0	25	15
3H-4, 33-34	20.84	7572	Volcaniclastic turbidite	98	St, sb, id (<1%)	<1	Biot, qz	0	2	<1	
3H-4, 35-36	20.86	7583	Volcaniclastic turbidite	35	95	St, sb, id (<5%)	<1	Qz, plag, amph	0	5	<1
3H-4, 49-50	21.00	7512	Volcaniclastic turbidite	98	St, sp, ip, id	<1	Qz, plag	<1	2	<1	
4H-2, 132-134	28.33	7508	Volcaniclastic turbidite	5	5	Sb, sp	90	Qz, biot, cpx, amph, tm	5	<1	80
4H-6, 6-7	33.07	7509	Tephra	2	<1	Sp	95	Kfsp, plag, biot, cpx	<1	5	85
7H-3, 82-84	57.83	7505	Tephra	5	98	Sb, sp (<1%), st (<1%)	2	Kfsp, plag, cpx, qz	<1	<1	15
7H-6, 20-22	61.71	7045	Tephra	99	Sb, st	<1	Kfsp	0	<1	20	
7H-6, 43-45	61.94	7046	Tephra	99	Sb, sp, st	<1	Qz, kfsp	0	<1	20	
9H-6, 99-100	81.50	7538	Volcaniclastic turbidite	85	Sb, sd, id (<1%)	<1	Cpx, plag, kfsp, qz	0	15	5	
9H-6, 120-121	81.71	7539	Volcaniclastic turbidite	90	Sb, sd	5	Kfsp, plag, cpx, amph, qz	0	5	30	
11H-7, 4-5	101.05	7502	Tephra	<1	60	Id	5	Cpx	0	35	40
13H-5, 44-45	117.45	7501	Tephra	2	70	Sd, sp	5	Kfsp, amph, biot	5	20	50

Note: Glass particle morphology: p = highly vesicular pumice, b = bubble wall shards, t = tubular pumice, d = dense to vesicle-poor shards. Color/composition: s = colorless/silicic, i = pale brown/intermediate, m = dark brown/mafic; * = percentages excluding zeolite aggregates. Mineral assemblage: kfsp = K-feldspar, plag = plagioclase, qz = quartz, cpx = clinopyroxene, amph = amphibole, biot = biotite, tm = titanomagnetite, sph = titanite.

Table 3. Statistics of rhyolite and basalt standard EMP analyses.

LIPARI						KN 18						
Reference	Mean	Min	Max	S.D.	Recovery	Reference	Mean	Min	Max	S.D.	Recovery	
SiO ₂	74.35	73.61	72.13	75.05	0.6	99	74.6	74.54	72.69	75.2	0.51	99.92
TiO ₂	0.09	0.05	0.13	0.02		0.18	0.19	0.11	0.24	0.03	105.56	
Al ₂ O ₃	12.87	12.86	12.6	13.07	0.11	99.92	10.53	10.62	10.33	10.83	0.11	100.86
FeO	1.51	1.48	1.3	1.65	0.07	98.01	3.45	3.4	3.13	3.84	0.13	98.55
MnO	0.07	0.07	0	0.14	0.03	100	0.06	0.06	0	0.13	0.03	100
MgO	0.05	0.04	0	0.08	0.02	80		0.01	0	0.03	0.01	
CaO	0.74	0.74	0.68	0.81	0.03	100	0.15	0.15	0.04	1.13	0.13	100
Na ₂ O	4.19	4.32	3.08	4.55	0.25	103.1	5.68	5.57	5.39	6	0.1	98.06
K ₂ O	5.11	5.09	4.59	5.33	0.13	99.61	4.39	4.41	2.72	4.67	0.35	100.46
P ₂ O ₅	0.02	0	0	0.08	0.02			0.02	0	0.06	0.02	
SO ₂	0.02	0	0	0.13	0.03			0.02	0	0.4	0.09	
ALV 981						JdF-D 2						
Reference	Mean	Min	Max	S.D.	Recovery	Reference	Mean	Min	Max	S.D.	Recovery	
SiO ₂	49.53	49.92	48.74	50.83	0.58	99.21	50.8	51.04	50.74	52.11	0.48	100.47
TiO ₂	1.27	1.27	1.22	1.34	0.04	100	1.93	1.91	1.86	2.08	0.08	98.96
Al ₂ O ₃	16.58	16.5	16.25	16.9	0.18	99.52	13.8	13.69	13.43	14.1	0.22	99.2
FeO	8.42	8.54	8.18	8.84	0.19	101.43	12.17	11.68	11.19	12.18	0.36	95.97
MnO	0.14	0.19	0.13	0.25	0.03	135.71	0.22	0.25	0.23	0.29	0.03	113.64
MgO	8.68	8.83	8.65	9.03	0.13	101.73	6.83	6.82	6.7	8.7	0.78	99.85
CaO	11.81	11.88	11.73	12	0.09	100.59	10.8	10.78	10.49	10.81	0.01	99.81
Na ₂ O	2.88	2.88	2.79	2.96	0.06	100	2.77	2.89	2.79	2.9	0.04	104.33
K ₂ O	0.05	0.05	0.03	0.07	0.01	100	0.22	0.2	0.18	0.22	0.01	90.91
P ₂ O ₅	0.06	0.15	0	0.22	0.07	250	0.23	0.26	0.08	0.3	0.08	113.04
SO ₂	0.05	0	0	0.1	0.04	0.33	0.29	0.37	0.04			

Note: S.D. = standard deviation. Data are in wt%.

sine function fit. Analytical errors are quoted as 1σ and include the uncertainties in the determination of blanks and the irradiation parameter J.

RESULTS

Petrography and Major-Element Composition of Glass Shards

According to their grain-size characteristics, internal sedimentary structures, sharp scoured contacts with underlying sediments, the abundance of glass shards and subhedral to euhedral volcanic crystals (40%–90%), and the admixture of shallow-water microfossils and nonvolcanic debris (10%–50%), most of the ash-bearing layers studied from Hole 974B (i.e., 7590, 7601, 7513, 7572 + 7583 + 7512, 7508, 7545 + 7546, and 7538 + 7539) represent volcaniclastic turbidites sensu lato, derived from the remobilization of subaerial and shal-

low-marine primary tephra layers (see McCoy and Cornell, 1990, for a comprehensive discussion of processes, definitions, and references). Depending on their predominant clastic components in the 63- to 250- μm grain-size fraction (Table 2), the ash-bearing layers are here divided into primary to slightly reworked vitric fallout tephra layers (tr), vitric volcaniclastic turbidite deposits (vt), and foraminiferous or crystal-lithic volcaniclastic sand layers (vs).

Sample tr-7501 (161-974B-13H-5, 44–45 cm)

Sample tr-7501 represents the oldest ash-bearing layer of Hole 974B in this study. Clastic components in the 2-cm-thick layer consist of >70 vol% of altered/hydrated, colorless, vesicle-poor to pumiceous, silicic glass shards (Fig. 2), ~5 vol% euhedral crystals (K-feldspar, amphibole, and biotite), ~5 vol% altered volcanic lithic clasts, and up to 20 vol% foraminifer shells. Abundant zeolite mineral aggregates indicate that its primary glass content may have been signif-

Table 4. Analyses of glasses from Hole 974B.

Core, section:	11H-7	11H-7	7H-3	7H-3	7H-3	7H-3	7H-3	7H-3
Interval:	4-5 cm	4-5 cm	82-84 cm	82-84 cm	82-84 cm	82-84 cm	82-84 cm	82-84 cm
Sample:	7502-1	7502-2	7505-1	7505-3	7505-4	7505-5	7505-6	7505-7
N:	2	3	3	3	3	3	3	2
SiO ₂	62.23 ± 0.22	62.12 ± 0.16	75.04 ± 0.13	72.29 ± 0.08	72.38 ± 0.19	72.52 ± 0.23	72.73 ± 0.01	72.28 ± 0.40
TiO ₂	0.81 ± 0.10	0.78 ± 0.05	0.15 ± 0.06	0.27 ± 0.03	0.24 ± 0.02	0.26 ± 0.02	0.23 ± 0.02	0.20 ± 0.02
Al ₂ O ₃	17.90 ± 0.09	18.00 ± 0.14	13.14 ± 0.08	14.18 ± 0.03	14.23 ± 0.02	14.31 ± 0.12	14.14 ± 0.03	14.32 ± 0.08
FeO	2.74 ± 0.17	2.74 ± 0.09	1.23 ± 0.08	1.31 ± 0.11	1.22 ± 0.04	1.30 ± 0.11	1.29 ± 0.09	1.32 ± 0.02
MnO	0.23 ± 0.01	0.22 ± 0.07	0.07 ± 0.02	0.10 ± 0.04	0.09 ± 0.03	0.06 ± 0.02	0.06 ± 0.03	0.11 ± 0.03
MgO	0.54 ± 0.03	0.49 ± 0.04	0.14 ± 0.02	0.17 ± 0.01	0.20 ± 0.01	0.21 ± 0.03	0.16 ± 0.01	0.20 ± 0.02
CaO	0.81 ± 0.01	0.79 ± 0.01	1.12 ± 0.04	0.94 ± 0.02	0.98 ± 0.04	1.00 ± 0.04	0.99 ± 0.04	1.01 ± 0.06
Na ₂ O	8.98 ± 0.20	9.13 ± 0.05	3.60 ± 0.09	4.19 ± 0.02	4.08 ± 0.11	3.99 ± 0.18	4.03 ± 0.06	4.00 ± 0.31
K ₂ O	5.29 ± 0.16	5.24 ± 0.00	5.31 ± 0.09	6.03 ± 0.08	6.01 ± 0.05	5.80 ± 0.06	5.85 ± 0.07	6.04 ± 0.03
P ₂ O ₅	0.14 ± 0.01	0.13 ± 0.02	0.04 ± 0.01	0.05 ± 0.02	0.05 ± 0.01	0.03 ± 0.01	0.07 ± 0.03	0.02 ± 0.01
SO ₂	0.08 ± 0.01	0.07 ± 0.04	0.04 ± 0.03	0.03 ± 0.02	0.03 ± 0.02	0.08 ± 0.00	0.02 ± 0.02	0.03 ± 0.02
Cl	0.15 ± 0.02	0.18 ± 0.02	0.08 ± 0.02	0.37 ± 0.03	0.40 ± 0.00	0.39 ± 0.02	0.37 ± 0.03	0.42 ± 0.02
F	0.08 ± 0.02	0.11 ± 0.01	0.06 ± 0.03	0.07 ± 0.04	0.09 ± 0.02	0.06 ± 0.02	0.05 ± 0.01	0.07 ± 0.02
Total:	97.23 ± 1.03	98.42 ± 0.57	93.50 ± 0.74	92.32 ± 0.18	91.83 ± 1.04	92.66 ± 0.19	90.42 ± 0.41	91.10 ± 0.01
Core, section:	7H-3							
Interval:	82-84 cm							
Sample:	7505-8	7505-9	7505-10	7505-11	7505-12	7505-13	7505-14	7505-15
N:	3	3	3	3	3	3	3	4
SiO ₂	72.18 ± 0.20	72.43 ± 0.11	72.52 ± 0.27	72.62 ± 0.10	72.20 ± 0.08	72.70 ± 0.07	72.45 ± 0.24	72.54 ± 0.09
TiO ₂	0.22 ± 0.02	0.22 ± 0.02	0.21 ± 0.01	0.23 ± 0.02	0.22 ± 0.04	0.21 ± 0.01	0.20 ± 0.00	0.24 ± 0.04
Al ₂ O ₃	14.27 ± 0.07	14.10 ± 0.09	14.09 ± 0.13	14.23 ± 0.05	14.31 ± 0.10	14.12 ± 0.07	14.04 ± 0.02	14.19 ± 0.04
FeO	1.39 ± 0.09	1.36 ± 0.08	1.33 ± 0.04	1.26 ± 0.05	1.31 ± 0.08	1.27 ± 0.12	1.29 ± 0.02	1.28 ± 0.09
MnO	0.07 ± 0.05	0.09 ± 0.03	0.07 ± 0.02	0.07 ± 0.05	0.05 ± 0.03	0.09 ± 0.05	0.11 ± 0.03	0.05 ± 0.03
MgO	0.21 ± 0.02	0.16 ± 0.02	0.18 ± 0.01	0.17 ± 0.02	0.20 ± 0.01	0.18 ± 0.01	0.20 ± 0.00	0.19 ± 0.02
CaO	1.01 ± 0.01	0.94 ± 0.07	0.96 ± 0.03	0.96 ± 0.02	1.00 ± 0.03	0.96 ± 0.05	0.97 ± 0.04	0.95 ± 0.04
Na ₂ O	4.24 ± 0.05	4.25 ± 0.08	4.10 ± 0.03	4.07 ± 0.01	4.15 ± 0.05	4.03 ± 0.02	4.22 ± 0.08	4.05 ± 0.04
K ₂ O	5.88 ± 0.08	5.96 ± 0.09	6.05 ± 0.03	5.91 ± 0.12	6.01 ± 0.18	5.95 ± 0.09	5.97 ± 0.18	5.98 ± 0.03
P ₂ O ₅	0.04 ± 0.03	0.01 ± 0.01	0.04 ± 0.04	0.06 ± 0.02	0.03 ± 0.03	0.02 ± 0.01	0.06 ± 0.01	0.04 ± 0.01
SO ₂	0.03 ± 0.03	0.03 ± 0.02	0.00 ± 0.01	0.03 ± 0.03	0.05 ± 0.06	0.02 ± 0.03	0.04 ± 0.01	0.04 ± 0.03
Cl	0.40 ± 0.02	0.37 ± 0.01	0.39 ± 0.02	0.35 ± 0.02	0.40 ± 0.03	0.38 ± 0.02	0.37 ± 0.04	0.37 ± 0.02
F	0.08 ± 0.01	0.08 ± 0.02	0.05 ± 0.04	0.05 ± 0.01	0.07 ± 0.02	0.07 ± 0.03	0.06 ± 0.02	0.09 ± 0.02
Total:	91.66 ± 0.38	92.96 ± 0.38	91.56 ± 0.47	90.93 ± 0.62	91.41 ± 0.42	91.60 ± 0.15	92.71 ± 0.65	91.95 ± 0.23
Core, section:	7H-3							
Interval:	82-84 cm							
Sample:	7505-17	7505-18	7505-19	7505-20	7505-21	7505-22	7505-23	7505-24
N:	3	3	3	3	3	3	2	1
SiO ₂	72.30 ± 0.19	72.37 ± 0.33	72.36 ± 0.04	72.20 ± 0.19	72.60 ± 0.13	72.52 ± 0.15	72.59 ± 0.14	72.33 ± 0.13
TiO ₂	0.22 ± 0.00	0.22 ± 0.03	0.21 ± 0.05	0.23 ± 0.00	0.21 ± 0.03	0.23 ± 0.03	0.23 ± 0.05	0.24 ± 0.05
Al ₂ O ₃	14.21 ± 0.08	14.22 ± 0.02	14.24 ± 0.04	14.33 ± 0.11	14.14 ± 0.05	14.23 ± 0.09	14.24 ± 0.07	14.15 ± 0.08
FeO	1.30 ± 0.06	1.29 ± 0.04	1.32 ± 0.02	1.37 ± 0.07	1.26 ± 0.05	1.29 ± 0.01	1.30 ± 0.06	1.36 ± 0.02
MnO	0.06 ± 0.04	0.07 ± 0.07	0.08 ± 0.01	0.06 ± 0.04	0.10 ± 0.04	0.09 ± 0.02	0.09 ± 0.03	0.08 ± 0.03
MgO	0.20 ± 0.02	0.20 ± 0.02	0.21 ± 0.01	0.22 ± 0.02	0.18 ± 0.02	0.18 ± 0.01	0.18 ± 0.01	0.20 ± 0.03
CaO	1.00 ± 0.04	0.93 ± 0.03	0.99 ± 0.03	1.02 ± 0.02	0.95 ± 0.03	0.97 ± 0.04	0.91 ± 0.02	0.97 ± 0.04
Na ₂ O	4.12 ± 0.04	4.29 ± 0.05	4.11 ± 0.04	4.04 ± 0.04	4.22 ± 0.05	4.19 ± 0.02	4.13 ± 0.03	4.18 ± 0.04
K ₂ O	6.10 ± 0.05	5.86 ± 0.17	5.92 ± 0.10	5.98 ± 0.02	5.82 ± 0.10	5.80 ± 0.10	5.84 ± 0.02	6.00 ± 0.05
P ₂ O ₅	0.04 ± 0.03	0.05 ± 0.02	0.05 ± 0.02	0.05 ± 0.04	0.04 ± 0.01	0.04 ± 0.02	0.02 ± 0.01	0.03 ± 0.02
SO ₂	0.02 ± 0.02	0.01 ± 0.01	0.07 ± 0.01	0.01 ± 0.03	0.05 ± 0.03	0.04 ± 0.03	0.02 ± 0.02	0.03 ± 0.03
Cl	0.38 ± 0.02	0.39 ± 0.01	0.39 ± 0.02	0.39 ± 0.04	0.37 ± 0.02	0.39 ± 0.02	0.36 ± 0.01	0.38 ± 0.01
F	0.05 ± 0.04	0.09 ± 0.03	0.07 ± 0.00	0.09 ± 0.04	0.05 ± 0.03	0.05 ± 0.03	0.09 ± 0.00	0.05 ± 0.01
Total:	91.43 ± 1.21	92.20 ± 0.71	91.91 ± 0.33	91.28 ± 0.67	92.33 ± 0.72	92.58 ± 0.61	91.88 ± 0.37	92.26 ± 0.75
Core, section:	9H-6							
Interval:	120-121 cm							
Sample:	7539-1	7539-2	7539-3	7539-4	7539-5	7539-6	7539-7	7539-9
N:	3	3	3	2	3	2	3	2
SiO ₂	75.97 ± 0.07	75.94 ± 0.25	74.42 ± 0.13	76.00 ± 0.16	74.35 ± 0.12	75.68 ± 0.08	76.29 ± 0.03	76.45 ± 0.07
TiO ₂	0.08 ± 0.03	0.10 ± 0.06	0.13 ± 0.02	0.09 ± 0.02	0.13 ± 0.01	0.09 ± 0.01	0.08 ± 0.01	0.09 ± 0.01
Al ₂ O ₃	12.73 ± 0.09	12.67 ± 0.09	13.28 ± 0.05	12.60 ± 0.14	13.45 ± 0.02	12.75 ± 0.16	12.88 ± 0.07	12.57 ± 0.09
FeO	1.19 ± 0.05	1.16 ± 0.05	1.18 ± 0.07	1.17 ± 0.00	1.24 ± 0.01	1.18 ± 0.03	1.12 ± 0.03	1.04 ± 0.03
MnO	0.07 ± 0.08	0.05 ± 0.03	0.13 ± 0.01	0.07 ± 0.02	0.10 ± 0.03	0.11 ± 0.04	0.07 ± 0.03	0.04 ± 0.02
MgO	0.01 ± 0.01	0.01 ± 0.01	0.04 ± 0.01	0.01 ± 0.01	0.04 ± 0.01	0.01 ± 0.01	0.02 ± 0.01	0.01 ± 0.01
CaO	0.47 ± 0.01	0.49 ± 0.02	0.56 ± 0.02	0.50 ± 0.05	0.58 ± 0.02	0.51 ± 0.00	0.46 ± 0.04	0.45 ± 0.02
Na ₂ O	4.11 ± 0.01	4.31 ± 0.06	4.65 ± 0.06	4.38 ± 0.02	4.41 ± 0.07	4.40 ± 0.19	3.98 ± 0.09	4.00 ± 0.04
K ₂ O	4.97 ± 0.20	4.93 ± 0.10	5.36 ± 0.06	4.85 ± 0.09	5.44 ± 0.07	4.96 ± 0.11	4.78 ± 0.02	5.07 ± 0.06
P ₂ O ₅	0.03 ± 0.03	0.01 ± 0.02	0.03 ± 0.02	0.01 ± 0.00	0.04 ± 0.03	0.01 ± 0.01	0.00 ± 0.00	0.03 ± 0.02
SO ₂	0.02 ± 0.02	0.02 ± 0.02	0.00 ± 0.00	0.01 ± 0.02	0.00 ± 0.01	0.01 ± 0.01	0.02 ± 0.04	0.01 ± 0.02
Cl	0.22 ± 0.02	0.21 ± 0.01	0.16 ± 0.01	0.20 ± 0.00	0.16 ± 0.01	0.20 ± 0.00	0.19 ± 0.02	0.18 ± 0.02
F	0.12 ± 0.04	0.09 ± 0.03	0.06 ± 0.03	0.11 ± 0.02	0.08 ± 0.06	0.10 ± 0.00	0.10 ± 0.01	0.06 ± 0.02
Total:	91.30 ± 0.27	93.14 ± 0.24	94.55 ± 0.66	93.42 ± 0.01	94.20 ± 0.65	93.62 ± 0.76	90.93 ± 0.57	92.22 ± 0.47

Table 4 (continued).

Core, section:	9H-6								
Interval:	120-121 cm								
Sample:	7539-11	7539-12	7539-14	7539-15	7539-16	7539-17	7539-18	7539-19	7539-20
N:	2	3	3	2	2	3	3	3	3
SiO ₂	76.45 ± 0.04	74.47 ± 0.17	76.43 ± 0.07	76.22 ± 0.10	76.50 ± 0.05	74.42 ± 0.21	74.66 ± 0.25	76.35 ± 0.07	76.31 ± 0.17
TiO ₂	0.07 ± 0.02	0.12 ± 0.05	0.10 ± 0.05	0.06 ± 0.06	0.09 ± 0.01	0.14 ± 0.01	0.12 ± 0.04	0.09 ± 0.04	0.06 ± 0.02
Al ₂ O ₃	12.86 ± 0.10	13.31 ± 0.07	12.70 ± 0.02	13.01 ± 0.04	12.86 ± 0.01	13.30 ± 0.09	13.28 ± 0.03	12.67 ± 0.03	12.78 ± 0.14
FeO	1.25 ± 0.10	1.34 ± 0.06	1.13 ± 0.06	1.09 ± 0.10	1.15 ± 0.10	1.31 ± 0.07	1.19 ± 0.09	1.09 ± 0.03	1.21 ± 0.02
MnO	0.07 ± 0.05	0.09 ± 0.01	0.08 ± 0.03	0.13 ± 0.04	0.02 ± 0.03	0.10 ± 0.05	0.09 ± 0.02	0.08 ± 0.01	0.08 ± 0.04
MgO	0.01 ± 0.02	0.03 ± 0.01	0.01 ± 0.01	0.01 ± 0.00	0.00 ± 0.00	0.03 ± 0.01	0.03 ± 0.01	0.01 ± 0.01	0.02 ± 0.01
CaO	0.46 ± 0.03	0.57 ± 0.03	0.47 ± 0.03	0.48 ± 0.01	0.43 ± 0.07	0.57 ± 0.01	0.53 ± 0.04	0.47 ± 0.04	0.46 ± 0.04
Na ₂ O	3.86 ± 0.01	4.62 ± 0.03	4.01 ± 0.06	3.97 ± 0.07	3.88 ± 0.03	4.60 ± 0.01	4.47 ± 0.15	3.98 ± 0.05	4.01 ± 0.08
K ₂ O	4.65 ± 0.02	5.21 ± 0.11	4.74 ± 0.09	4.74 ± 0.10	4.73 ± 0.00	5.24 ± 0.07	5.36 ± 0.25	4.96 ± 0.11	4.73 ± 0.16
P ₂ O ₅	0.01 ± 0.01	0.03 ± 0.01	0.01 ± 0.01	0.04 ± 0.00	0.03 ± 0.01	0.03 ± 0.01	0.03 ± 0.02	0.02 ± 0.01	0.03 ± 0.02
SO ₂	0.02 ± 0.02	0.01 ± 0.02	0.00 ± 0.01	0.00 ± 0.00	0.02 ± 0.02	0.01 ± 0.01	0.01 ± 0.02	0.01 ± 0.03	0.03 ± 0.02
Cl	0.20 ± 0.02	0.15 ± 0.01	0.20 ± 0.01	0.19 ± 0.01	0.19 ± 0.01	0.17 ± 0.03	0.19 ± 0.02	0.20 ± 0.02	0.19 ± 0.02
F	0.09 ± 0.02	0.05 ± 0.03	0.11 ± 0.02	0.07 ± 0.02	0.09 ± 0.02	0.07 ± 0.03	0.05 ± 0.02	0.07 ± 0.02	0.09 ± 0.03
Total:	90.84 ± 0.69	94.81 ± 0.42	90.67 ± 0.68	90.47 ± 0.53	90.78 ± 0.52	94.33 ± 0.39	95.01 ± 0.36	91.82 ± 0.26	90.72 ± 0.26
Core, section:	9H-6								
Interval:	120-121 cm								
Sample:	7539-21	7539-22	7539-23	7539-25	7539-26	7539-13			
N:	3	3	3	3	2	1			
SiO ₂	76.11 ± 0.19	76.42 ± 0.28	74.87 ± 0.24	76.01 ± 0.13	76.31 ± 0.00	76.62			
TiO ₂	0.08 ± 0.02	0.10 ± 0.03	0.09 ± 0.01	0.07 ± 0.03	0.09 ± 0.05	0.10			
Al ₂ O ₃	12.61 ± 0.11	12.72 ± 0.09	13.18 ± 0.06	12.50 ± 0.17	12.72 ± 0.10	12.99			
FeO	1.12 ± 0.02	1.09 ± 0.03	1.24 ± 0.07	1.25 ± 0.10	1.20 ± 0.11	1.28			
MnO	0.14 ± 0.03	0.09 ± 0.02	0.08 ± 0.02	0.08 ± 0.01	0.05 ± 0.01	0.12			
MgO	0.00 ± 0.01	0.01 ± 0.01	0.03 ± 0.01	0.00 ± 0.00	0.01 ± 0.01	0.01			
CaO	0.46 ± 0.03	0.46 ± 0.02	0.53 ± 0.01	0.54 ± 0.01	0.48 ± 0.01	0.48			
Na ₂ O	4.11 ± 0.03	4.00 ± 0.07	4.43 ± 0.10	4.13 ± 0.07	3.98 ± 0.05	3.70			
K ₂ O	5.00 ± 0.09	4.77 ± 0.11	5.26 ± 0.19	5.06 ± 0.08	4.84 ± 0.09	4.38			
P ₂ O ₅	0.02 ± 0.02	0.02 ± 0.02	0.02 ± 0.02	0.02 ± 0.02	0.02 ± 0.02	0.03			
SO ₂	0.00 ± 0.00	0.02 ± 0.02	0.01 ± 0.01	0.04 ± 0.03	0.01 ± 0.00	0.03			
Cl	0.20 ± 0.01	0.20 ± 0.01	0.16 ± 0.00	0.19 ± 0.01	0.20 ± 0.02	0.18			
F	0.14 ± 0.01	0.11 ± 0.01	0.08 ± 0.02	0.11 ± 0.04	0.10 ± 0.01	0.08			
Total:	91.32 ± 1.03	90.55 ± 0.40	93.09 ± 0.53	90.91 ± 0.68	91.61 ± 0.74	90.05			
Core, section:	9H-6								
Interval:	99-100 cm								
Sample:	7538-1	7538-3	7538-4	7538-6	7538-7	7538-8	7538-9	7538-10	7538-11
N:	3	4	4	2	3	3	2	3	4
SiO ₂	76.65 ± 0.07	76.15 ± 0.15	76.08 ± 0.14	74.54 ± 0.03	74.38 ± 0.15	76.25 ± 0.19	76.11 ± 0.20	75.86 ± 0.21	76.01 ± 0.11
TiO ₂	0.05 ± 0.02	0.07 ± 0.01	0.09 ± 0.03	0.13 ± 0.00	0.12 ± 0.01	0.11 ± 0.02	0.10 ± 0.01	0.08 ± 0.05	0.11 ± 0.04
Al ₂ O ₃	12.95 ± 0.02	12.84 ± 0.14	12.82 ± 0.08	13.45 ± 0.02	13.55 ± 0.06	12.86 ± 0.14	12.69 ± 0.10	12.71 ± 0.12	12.87 ± 0.10
FeO	1.10 ± 0.03	1.18 ± 0.12	1.16 ± 0.08	1.18 ± 0.09	1.21 ± 0.06	1.20 ± 0.06	1.12 ± 0.02	1.14 ± 0.12	1.15 ± 0.06
MnO	0.07 ± 0.06	0.05 ± 0.02	0.07 ± 0.04	0.11 ± 0.04	0.16 ± 0.05	0.09 ± 0.01	0.09 ± 0.05	0.08 ± 0.02	0.08 ± 0.06
MgO	0.01 ± 0.00	0.01 ± 0.01	0.01 ± 0.01	0.02 ± 0.01	0.04 ± 0.01	0.01 ± 0.01	0.00 ± 0.00	0.01 ± 0.02	0.01 ± 0.02
CaO	0.48 ± 0.02	0.46 ± 0.03	0.47 ± 0.03	0.56 ± 0.01	0.53 ± 0.01	0.49 ± 0.04	0.47 ± 0.01	0.50 ± 0.01	0.50 ± 0.03
Na ₂ O	3.77 ± 0.03	4.06 ± 0.03	4.16 ± 0.04	4.42 ± 0.04	4.42 ± 0.06	3.82 ± 0.04	4.10 ± 0.01	4.58 ± 0.06	4.00 ± 0.02
K ₂ O	4.58 ± 0.08	4.85 ± 0.07	4.85 ± 0.11	5.27 ± 0.09	5.31 ± 0.18	4.83 ± 0.11	4.97 ± 0.06	4.74 ± 0.07	4.94 ± 0.04
P ₂ O ₅	0.02 ± 0.02	0.02 ± 0.01	0.02 ± 0.02	0.03 ± 0.02	0.03 ± 0.02	0.01 ± 0.01	0.00 ± 0.00	0.01 ± 0.02	0.01 ± 0.01
SO ₂	0.01 ± 0.02	0.01 ± 0.02	0.01 ± 0.01	0.04 ± 0.02	0.00 ± 0.00	0.02 ± 0.02	0.04 ± 0.02	0.01 ± 0.01	0.02 ± 0.02
Cl	0.20 ± 0.04	0.18 ± 0.02	0.18 ± 0.01	0.16 ± 0.01	0.16 ± 0.02	0.20 ± 0.01	0.21 ± 0.02	0.18 ± 0.02	0.19 ± 0.02
F	0.11 ± 0.01	0.12 ± 0.03	0.08 ± 0.02	0.08 ± 0.04	0.09 ± 0.05	0.10 ± 0.02	0.09 ± 0.01	0.10 ± 0.03	0.10 ± 0.03
Total:	90.49 ± 0.32	92.13 ± 0.38	92.27 ± 0.51	94.91 ± 0.33	94.78 ± 0.61	91.71 ± 1.03	92.70 ± 0.59	94.34 ± 1.56	91.93 ± 0.51
Core, section:	9H-6								
Interval:	99-100	99-100	99-100	99-100	99-100	99-100	99-100	99-100	99-100
Sample:	7538-12	7538-13	7538-14	7538-15	7538-16	7538-18	7538-20	7538-21	7538-22
N:	2	2	2	2	3	2	3	3	3
SiO ₂	75.59 ± 1.69	74.47 ± 0.12	76.27 ± 0.17	76.40 ± 0.12	75.88 ± 0.09	76.38 ± 0.21	76.19 ± 0.16	76.08 ± 0.15	74.72 ± 0.30
TiO ₂	0.14 ± 0.03	0.12 ± 0.04	0.12 ± 0.04	0.13 ± 0.05	0.09 ± 0.03	0.11 ± 0.01	0.10 ± 0.01	0.06 ± 0.03	0.11 ± 0.02
Al ₂ O ₃	13.53 ± 0.12	13.44 ± 0.13	12.83 ± 0.05	12.93 ± 0.14	12.87 ± 0.02	12.76 ± 0.07	12.67 ± 0.12	12.70 ± 0.11	13.14 ± 0.09
FeO	1.29 ± 0.14	1.24 ± 0.03	1.16 ± 0.07	1.16 ± 0.05	1.09 ± 0.09	1.08 ± 0.08	1.11 ± 0.05	1.09 ± 0.03	1.25 ± 0.10
MnO	0.13 ± 0.03	0.06 ± 0.00	0.08 ± 0.02	0.11 ± 0.09	0.12 ± 0.02	0.12 ± 0.04	0.05 ± 0.04	0.08 ± 0.03	0.10 ± 0.08
MgO	0.03 ± 0.03	0.03 ± 0.01	0.01 ± 0.00	0.01 ± 0.02	0.00 ± 0.00	0.01 ± 0.02	0.00 ± 0.01	0.03 ± 0.01	0.04 ± 0.01
CaO	0.54 ± 0.02	0.62 ± 0.03	0.47 ± 0.09	0.47 ± 0.01	0.50 ± 0.01	0.46 ± 0.01	0.48 ± 0.04	0.46 ± 0.04	0.51 ± 0.02
Na ₂ O	3.11 ± 1.60	4.47 ± 0.00	3.99 ± 0.02	3.85 ± 0.04	4.10 ± 0.01	3.96 ± 0.04	4.10 ± 0.11	4.27 ± 0.00	4.14 ± 0.19
K ₂ O	5.33 ± 0.39	5.26 ± 0.09	4.78 ± 0.10	4.58 ± 0.07	5.02 ± 0.08	4.76 ± 0.06	5.00 ± 0.16	4.89 ± 0.15	5.67 ± 0.05
P ₂ O ₅	0.03 ± 0.03	0.02 ± 0.02	0.02 ± 0.02	0.04 ± 0.02	0.03 ± 0.01	0.01 ± 0.02	0.02 ± 0.02	0.03 ± 0.02	0.04 ± 0.03
SO ₂	0.00 ± 0.00	0.00 ± 0.00	0.00 ± 0.00	0.03 ± 0.02	0.00 ± 0.01	0.04 ± 0.02	0.01 ± 0.01	0.03 ± 0.01	0.01 ± 0.01
Cl	0.20 ± 0.02	0.18 ± 0.00	0.17 ± 0.01	0.20 ± 0.00	0.21 ± 0.02	0.20 ± 0.00	0.18 ± 0.01	0.18 ± 0.03	0.17 ± 0.02
F	0.08 ± 0.01	0.08 ± 0.02	0.10 ± 0.02	0.08 ± 0.01	0.09 ± 0.03	0.10 ± 0.05	0.09 ± 0.04	0.10 ± 0.03	0.08 ± 0.02
Total:	92.15 ± 0.85	94.14 ± 0.15	90.99 ± 0.17	90.71 ± 0.23	91.51 ± 0.31	90.99 ± 1.36	91.74 ± 0.28	92.58 ± 0.38	93.91 ± 0.71

Table 4 (continued).

Core, section:	9H-6							
Interval:	99-100	99-100	99-100	99-100	99-100	99-100	99-100	99-100
Sample:	7538-23	7538-25	7538-27	7538-5	7538-17	7538-19	7538-24	7538-26
N:	3	3	2	1	1	1	1	1
SiO ₂	76.43 ± 0.10	76.25 ± 0.04	74.43 ± 0.18	76.26	76.20	76.70	74.84	77.12
TiO ₂	0.11 ± 0.04	0.08 ± 0.02	0.13 ± 0.02	0.03	0.12	0.07	0.13	0.10
Al ₂ O ₃	12.78 ± 0.09	12.74 ± 0.01	13.21 ± 0.02	12.70	12.80	13.11	13.71	12.84
FeO	1.17 ± 0.04	1.19 ± 0.04	1.26 ± 0.13	1.18	1.16	1.03	1.16	1.12
MnO	0.12 ± 0.03	0.11 ± 0.02	0.04 ± 0.02	0.09	0.04	0.04	0.10	0.00
MgO	0.02 ± 0.01	0.01 ± 0.01	0.03 ± 0.00	0.01	0.03	0.00	0.02	0.01
CaO	0.47 ± 0.03	0.48 ± 0.01	0.52 ± 0.01	0.51	0.46	0.45	0.74	0.50
Na ₂ O	3.87 ± 0.04	3.95 ± 0.04	4.53 ± 0.05	3.86	3.93	3.75	4.76	3.59
K ₂ O	4.71 ± 0.08	4.92 ± 0.02	5.57 ± 0.11	4.95	4.87	4.52	4.31	4.38
P ₂ O ₅	0.04 ± 0.03	0.01 ± 0.01	0.01 ± 0.01	0.06	0.03	0.02	0.00	0.02
SO ₂	0.00 ± 0	0.01 ± 0.02	0.01 ± 0.01	0.02	0.01	0.02	0.00	0.01
Cl	0.18 ± 0.01	0.19 ± 0.01	0.19 ± 0.04	0.19	0.21	0.20	0.13	0.21
F	0.10 ± 0.03	0.07 ± 0.02	0.09 ± 0.02	0.15	0.13	0.09	0.09	0.10
Total:	90.89 ± 0.45	91.2 ± 0.70	94.32 ± 0.04	90.74	90.42	91.14	91.39	90.25
Core, section:	3H-4	3H-4	3H-4	3H-4	3H-4	2H-4	2H-4	2H-4
Interval:	49-50 cm	35-38 cm	35-38 cm	35-38 cm				
Sample:	7512-2	7512-4	7512-5	7512-6	7512-1	7513-1	7513-2	7513-3
N:	2	3	2	3	1	3	2	3
SiO ₂	70.56 ± 0.17	70.70 ± 0.06	70.44 ± 0.16	58.01 ± 0.08	72.41	61.10 ± 0.34	60.70 ± 0.14	62.08 ± 0.33
TiO ₂	0.58 ± 0.01	0.61 ± 0.02	0.63 ± 0.03	1.22 ± 0.05	0.24	0.60 ± 0.01	0.32 ± 0.07	0.62 ± 0.05
Al ₂ O ₃	13.80 ± 0.16	13.79 ± 0.04	13.79 ± 0.02	15.25 ± 0.15	14.23	18.47 ± 0.12	19.26 ± 0.20	18.00 ± 0.08
FeO	3.48 ± 0.09	3.47 ± 0.16	3.43 ± 0.10	9.01 ± 0.15	1.21	2.47 ± 0.09	1.96 ± 0.02	2.48 ± 0.08
MnO	0.14 ± 0.01	0.17 ± 0.07	0.15 ± 0.02	0.20 ± 0.02	0.10	0.20 ± 0.06	0.23 ± 0.01	0.21 ± 0.03
MgO	0.64 ± 0.01	0.59 ± 0.02	0.60 ± 0.02	3.01 ± 0.06	0.22	0.37 ± 0.03	0.19 ± 0.02	0.40 ± 0.03
CaO	2.40 ± 0.08	2.34 ± 0.05	2.36 ± 0.05	6.65 ± 0.10	1.05	1.31 ± 0.04	2.07 ± 0.02	1.28 ± 0.02
Na ₂ O	4.17 ± 0.29	4.31 ± 0.07	4.44 ± 0.03	3.78 ± 0.12	4.18	7.92 ± 0.08	5.90 ± 0.11	7.33 ± 0.05
K ₂ O	3.56 ± 0.02	3.48 ± 0.06	3.61 ± 0.09	2.21 ± 0.03	5.84	6.88 ± 0.24	8.79 ± 0.35	6.87 ± 0.11
P ₂ O ₅	0.13 ± 0.03	0.12 ± 0.03	0.11 ± 0.01	0.31 ± 0.03	0.03	0.06 ± 0.03	0.03 ± 0.03	0.08 ± 0.01
SO ₂	0.05 ± 0.02	0.01 ± 0.02	0.01 ± 0.01	0.10 ± 0.03	0.00	0.09 ± 0.02	0.13 ± 0.05	0.07 ± 0.04
Cl	0.40 ± 0.02	0.32 ± 0.01	0.35 ± 0.04	0.18 ± 0.03	0.39	0.37 ± 0.01	0.10 ± 0.02	0.37 ± 0.06
F	0.08 ± 0.06	0.10 ± 0.02	0.08 ± 0.02	0.06 ± 0.05	0.10	0.17 ± 0.03	0.32 ± 0.09	0.19 ± 0.02
Total:	91.98 ± 1.38	93.59 ± 0.13	92.63 ± 0.30	94.69 ± 0.22	92.39	96.61 ± 0.45	92.99 ± 0.59	91.66 ± 0.67
Core, section:	7H-6	7H-6	7H-6	3H-4	1H-3	1H-3	1H-3	1H-3
Interval:	20-22 cm	43-45 cm	43-45 cm	33-34 cm	57-58 cm	57-58 cm	57-58 cm	57-58 cm
Sample:	7545-1	7546-1	7546-2	7572-1	7590-1	7590-2	7590-3	7590-5
N:	1	1	1	1	2	3	2	1
SiO ₂	70.02	66.83	72.15	70.15	60.02 ± 0.21	53.40 ± 0.33	60.53 ± 0.08	57.83 ± 0.08
TiO ₂	0.51	0.57	0.15	0.65	0.51 ± 0.08	1.51 ± 0.03	0.46 ± 0.01	0.71 ± 0.04
Al ₂ O ₃	14.70	15.96	14.19	13.21	18.59 ± 0.07	17.72 ± 0.33	18.91 ± 0.05	19.04 ± 0.24
FeO	2.24	2.78	2.09	3.47	3.71 ± 0.12	8.37 ± 0.10	3.33 ± 0.17	4.57 ± 0.66
MnO	0.10	0.13	0.16	0.12	0.13 ± 0.01	0.17 ± 0.03	0.17 ± 0.01	0.16 ± 0.04
MgO	0.45	0.56	0.07	0.59	1.01 ± 0.03	3.23 ± 0.03	0.63 ± 0.04	1.42 ± 0.21
CaO	1.47	2.09	0.63	2.78	3.80 ± 0.06	7.22 ± 0.12	2.53 ± 0.08	3.58 ± 0.34
Na ₂ O	4.29	4.98	4.96	4.17	2.82 ± 0.11	3.89 ± 0.06	4.95 ± 0.02	4.54 ± 0.13
K ₂ O	5.56	5.44	5.24	4.36	9.10 ± 0.03	4.20 ± 0.04	7.67 ± 0.09	6.67 ± 0.21
P ₂ O ₅	0.10	0.15	0.06	0.12	0.00 ± 0.00	0.00 ± 0.00	0.00 ± 0.00	0.00 ± 0.00
SO ₂	0.02	0.00	0.01	0.01	0.00 ± 0.00	0.00 ± 0.00	0.00 ± 0.00	0.00 ± 0.00
Cl	0.44	0.42	0.21	0.30	0.03 ± 0.03	0.12 ± 0.01	0.59 ± 0.02	0.40 ± 0.02
F	0.10	0.12	0.07	0.07	0.26 ± 0.00	0.16 ± 0.03	0.23 ± 0.01	1.09 ± 1.28
Total:	92.69	95.47	94.11	94.23	96.30 ± 0.11	98.68 ± 0.33	99.95 ± 0.13	99.78 ± 0.85
Core, section:	3H-4							
Interval:	35-36 cm							
Sample:	7583-6	7583-8	7583-9	7583-10	7583-11	7583-12	7583-13	7583-14
N:	3	2	2	3	2	3	2	3
SiO ₂	70.65 ± 0.25	72.78 ± 0.26	72.79 ± 0.19	64.60 ± 0.14	72.83 ± 0.01	62.00 ± 0.19	72.96 ± 0.10	72.94 ± 0.03
TiO ₂	0.55 ± 0.05	0.46 ± 0.05	0.45 ± 0.08	0.70 ± 0.03	0.54 ± 0.02	0.77 ± 0.02	0.48 ± 0.01	0.45 ± 0.03
Al ₂ O ₃	14.18 ± 0.11	13.87 ± 0.05	13.78 ± 0.07	15.29 ± 0.34	13.92 ± 0.04	15.74 ± 0.14	13.62 ± 0.09	13.90 ± 0.05
FeO	4.39 ± 0.05	3.57 ± 0.08	3.66 ± 0.04	7.17 ± 0.15	3.65 ± 0.02	8.79 ± 0.06	3.57 ± 0.04	3.60 ± 0.12
MnO	0.14 ± 0.02	0.14 ± 0.04	0.11 ± 0.03	0.18 ± 0.04	0.13 ± 0.04	0.21 ± 0.01	0.16 ± 0.02	0.13 ± 0.05
MgO	1.02 ± 0.04	0.62 ± 0.07	0.60 ± 0.00	2.30 ± 0.09	0.63 ± 0.03	2.99 ± 0.06	0.66 ± 0.00	0.64 ± 0.02
CaO	1.89 ± 0.08	1.41 ± 0.02	1.42 ± 0.09	3.42 ± 0.09	1.41 ± 0.00	3.96 ± 0.02	1.45 ± 0.01	1.47 ± 0.05
Na ₂ O	4.53 ± 0.07	4.44 ± 0.02	4.45 ± 0.05	4.08 ± 0.04	4.20 ± 0.00	3.63 ± 0.04	4.41 ± 0.06	4.30 ± 0.05
K ₂ O	2.09 ± 0.04	2.25 ± 0.03	2.27 ± 0.11	1.46 ± 0.02	2.23 ± 0.04	1.23 ± 0.03	2.27 ± 0.04	2.20 ± 0.03
P ₂ O ₅	0.21 ± 0.01	0.16 ± 0.00	0.14 ± 0.02	0.49 ± 0.03	0.12 ± 0.02	0.35 ± 0.02	0.12 ± 0.02	0.14 ± 0.01
SO ₂	0.05 ± 0.02	0.04 ± 0.05	0.03 ± 0.02	0.09 ± 0.03	0.02 ± 0.02	0.11 ± 0.03	0.03 ± 0.04	0.01 ± 0.02
Cl	0.19 ± 0.01	0.21 ± 0.01	0.20 ± 0.02	0.13 ± 0.03	0.21 ± 0.03	0.13 ± 0.02	0.18 ± 0.01	0.16 ± 0.02
F	0.11 ± 0.01	0.05 ± 0.08	0.09 ± 0.03	0.09 ± 0.03	0.12 ± 0.01	0.08 ± 0.02	0.09 ± 0.03	0.06 ± 0.03
Total:	91.67 ± 0.95	91.58 ± 0.04	91.01 ± 0.64	92.83 ± 1.00	90.62 ± 0.21	92.21 ± 1.07	91.14 ± 0.13	91.26 ± 0.20

Table 4 (continued).

Core, section:	3H-4								
Interval:	35-36 cm								
Sample:	7583-16	7583-17	7583-18	7583-19	7583-20	7583-1	7583-3	7583-4	7583-7
N:	2	2	2	3	3	1	1	1	1
SiO ₂	63.13 ± 0.03	64.92 ± 1.46	73.52 ± 1.68	72.19 ± 0.64	72.83 ± 0.19	73.78	72.61	73.83	63.48
TiO ₂	0.74 ± 0.00	0.72 ± 0.05	0.51 ± 0.03	0.46 ± 0.08	0.48 ± 0.06	0.35	0.39	0.34	0.76
Al ₂ O ₃	15.45 ± 0.01	15.38 ± 0.34	13.94 ± 0.35	13.92 ± 0.12	13.77 ± 0.09	13.88	14.17	13.83	15.48
FeO	7.97 ± 0.05	7.17 ± 1.12	3.76 ± 0.08	3.88 ± 0.26	3.62 ± 0.07	3.97	4.60	3.54	7.48
MnO	0.17 ± 0.08	0.14 ± 0.04	0.22 ± 0.04	0.19 ± 0.05	0.14 ± 0.02	0.17	0.20	0.17	0.20
MgO	2.77 ± 0.04	2.64 ± 0.90	0.63 ± 0.01	0.74 ± 0.06	0.64 ± 0.03	0.59	0.63	0.59	2.55
CaO	3.80 ± 0.07	3.44 ± 0.39	1.56 ± 0.06	1.59 ± 0.15	1.41 ± 0.07	0.96	1.18	1.12	3.73
Na ₂ O	3.85 ± 0.00	3.35 ± 1.14	3.18 ± 1.97	4.41 ± 0.05	4.37 ± 0.10	4.36	4.17	4.53	4.02
K ₂ O	1.35 ± 0.03	1.49 ± 0.19	2.24 ± 0.09	2.18 ± 0.08	2.33 ± 0.05	1.62	1.77	1.61	1.47
P ₂ O ₅	0.49 ± 0.01	0.45 ± 0.05	0.14 ± 0.07	0.15 ± 0.02	0.13 ± 0.02	0.09	0.10	0.18	0.45
SO ₂	0.07 ± 0.01	0.07 ± 0.02	0.01 ± 0.01	0.00 ± 0.00	0.02 ± 0.02	0.00	0.00	0.04	0.17
Cl	0.12 ± 0.02	0.15 ± 0.00	0.23 ± 0.01	0.21 ± 0.04	0.20 ± 0.01	0.11	0.12	0.16	0.14
F	0.09 ± 0.02	0.08 ± 0.01	0.08 ± 0.01	0.09 ± 0.02	0.08 ± 0.03	0.12	0.07	0.06	0.05
Total:	92.91 ± 0.06	91.64 ± 1.43	90.94 ± 1.02	90.87 ± 0.69	91.03 ± 0.69	90.40	90.21	90.07	93.26
Core, section:	2H-3								
Interval:	22-23 cm								
Sample:	7600-1	7600-2	7600-3	7600-4	7600-5	7600-9	7600-11	7600-12	7600-6
N:	6	2	2	3	2	2	3	3	1
SiO ₂	61.33 ± 0.73	57.09 ± 0.31	62.06 ± 0.09	61.33 ± 0.17	61.45 ± 0.13	61.93 ± 0.10	61.34 ± 0.87	61.30 ± 0.13	61.43
TiO ₂	0.50 ± 0.05	0.62 ± 0.02	0.60 ± 0.07	0.48 ± 0.04	0.48 ± 0.03	0.49 ± 0.02	0.53 ± 0.03	0.47 ± 0.03	0.54
Al ₂ O ₃	18.81 ± 0.38	19.51 ± 0.88	17.97 ± 0.13	18.93 ± 0.16	17.96 ± 0.19	17.79 ± 0.00	18.59 ± 0.23	18.56 ± 0.14	17.87
FeO	2.64 ± 0.26	4.11 ± 0.49	2.72 ± 0.08	2.16 ± 0.11	2.88 ± 0.01	2.68 ± 0.07	2.50 ± 0.03	2.36 ± 0.03	2.77
MnO	0.15 ± 0.02	0.13 ± 0.04	0.14 ± 0.10	0.16 ± 0.07	0.09 ± 0.00	0.09 ± 0.01	0.17 ± 0.01	0.16 ± 0.01	0.22
MgO	0.50 ± 0.11	1.03 ± 0.43	0.57 ± 0.03	0.27 ± 0.02	0.65 ± 0.01	0.69 ± 0.03	0.39 ± 0.03	0.35 ± 0.06	0.67
CaO	2.54 ± 0.15	4.73 ± 0.40	2.44 ± 0.06	2.28 ± 0.03	2.56 ± 0.06	2.51 ± 0.04	2.49 ± 0.04	2.39 ± 0.03	2.68
Na ₂ O	3.19 ± 0.39	3.12 ± 0.53	3.81 ± 0.02	4.60 ± 0.16	3.44 ± 0.02	3.33 ± 0.24	4.03 ± 0.79	4.39 ± 0.05	3.70
K ₂ O	9.82 ± 0.59	8.84 ± 0.15	9.26 ± 0.20	9.37 ± 0.10	9.89 ± 0.08	9.95 ± 0.36	9.36 ± 0.28	9.58 ± 0.10	9.56
P ₂ O ₅	0.04 ± 0.03	0.16 ± 0.15	0.10 ± 0.05	0.07 ± 0.01	0.13 ± 0.00	0.14 ± 0.02	0.07 ± 0.01	0.05 ± 0.03	0.13
SO ₂	0.14 ± 0.08	0.35 ± 0.14	0.07 ± 0.01	0.06 ± 0.06	0.22 ± 0.03	0.21 ± 0.02	0.20 ± 0.05	0.13 ± 0.05	0.13
Cl	0.07 ± 0.02	0.06 ± 0.02	0.05 ± 0.01	0.06 ± 0.02	0.09 ± 0.05	0.06 ± 0.01	0.07 ± 0.01	0.06 ± 0.01	0.12
F	0.27 ± 0.07	0.25 ± 0.03	0.21 ± 0.01	0.22 ± 0.03	0.16 ± 0.03	0.13 ± 0.04	0.23 ± 0.01	0.20 ± 0.03	0.17
Total:	96.81 ± 1.20	96.60 ± 1.83	94.91 ± 0.09	93.76 ± 0.23	92.12 ± 2.04	92.60 ± 0.20	94.78 ± 0.82	97.34 ± 0.29	92.14
Core, section:	2H-1								
Interval:	37-38 cm								
Sample:	7601-1	7601-2	7601-3	7601-5	7601-6	7601-7	7601-8	7601-9	7601-10
N:	2	3	2	2	2	2	2	2	2
SiO ₂	57.33 ± 0.30	54.92 ± 0.29	57.38 ± 0.44	59.96 ± 0.12	62.92 ± 0.13	60.70 ± 0.03	61.37 ± 0.05	59.98 ± 0.11	63.91 ± 0.57
TiO ₂	0.69 ± 0.01	1.43 ± 0.14	0.69 ± 0.03	0.64 ± 0.07	0.45 ± 0.02	0.58 ± 0.01	0.58 ± 0.03	0.56 ± 0.08	0.46 ± 0.02
Al ₂ O ₃	18.70 ± 0.02	17.70 ± 0.06	18.65 ± 0.11	19.08 ± 0.03	19.28 ± 0.09	18.73 ± 0.03	18.75 ± 0.05	18.71 ± 0.04	17.56 ± 0.22
FeO	4.79 ± 0.13	6.85 ± 0.30	4.81 ± 0.15	3.55 ± 0.10	2.18 ± 0.11	3.33 ± 0.15	3.09 ± 0.01	3.62 ± 0.13	2.34 ± 0.17
MnO	0.18 ± 0.04	0.15 ± 0.03	0.19 ± 0.01	0.19 ± 0.01	0.15 ± 0.06	0.13 ± 0.04	0.14 ± 0.04	0.16 ± 0.04	0.13 ± 0.05
MgO	1.54 ± 0.03	2.61 ± 0.05	1.53 ± 0.07	0.93 ± 0.02	0.39 ± 0.00	0.92 ± 0.05	0.76 ± 0.00	1.01 ± 0.06	0.37 ± 0.04
CaO	4.67 ± 0.18	5.87 ± 0.07	4.66 ± 0.06	3.36 ± 0.12	1.92 ± 0.08	3.01 ± 0.03	2.62 ± 0.00	3.23 ± 0.16	1.86 ± 0.01
Na ₂ O	4.48 ± 0.07	3.60 ± 0.08	4.35 ± 0.09	4.21 ± 0.08	4.98 ± 0.09	4.57 ± 0.01	4.30 ± 0.04	4.80 ± 0.00	5.87 ± 0.10
K ₂ O	6.42 ± 0.01	5.67 ± 0.13	6.46 ± 0.01	7.12 ± 0.01	7.06 ± 0.10	7.02 ± 0.25	7.76 ± 0.01	6.95 ± 0.09	6.78 ± 0.09
P ₂ O ₅	0.28 ± 0.03	0.65 ± 0.04	0.38 ± 0.03	0.18 ± 0.00	0.04 ± 0.01	0.14 ± 0.01	0.12 ± 0.02	0.18 ± 0.03	0.09 ± 0.05
SO ₂	0.31 ± 0.05	0.07 ± 0.03	0.31 ± 0.13	0.15 ± 0.07	0.06 ± 0.04	0.15 ± 0.02	0.07 ± 0.04	0.22 ± 0.00	0.06 ± 0.01
Cl	0.41 ± 0.02	0.22 ± 0.03	0.39 ± 0.04	0.40 ± 0.04	0.30 ± 0.02	0.51 ± 0.01	0.29 ± 0.02	0.42 ± 0.00	0.37 ± 0.02
F	0.19 ± 0.11	0.26 ± 0.02	0.21 ± 0.01	0.24 ± 0.02	0.26 ± 0.03	0.20 ± 0.03	0.15 ± 0.02	0.18 ± 0.01	0.19 ± 0.01
Total:	96.90 ± 1.34	99.06 ± 0.65	98.04 ± 0.88	94.32 ± 0.54	95.44 ± 0.13	95.22 ± 0.05	95.49 ± 0.62	96.54 ± 0.53	92.39 ± 0.04
Core, section:	2H-1								
Interval:	37-38 cm								
Sample:	7601-11	7601-12	7601-13	7601-14	7601-15	7601-16	7601-17	7601-18	7601-19
N:	3	3	3	3	3	3	3	2	3
SiO ₂	61.83 ± 0.03	63.22 ± 1.95	69.49 ± 0.15	62.10 ± 0.18	62.56 ± 0.09	62.00 ± 0.16	59.07 ± 2.79	64.08 ± 2.55	61.88 ± 0.15
TiO ₂	0.64 ± 0.05	0.64 ± 0.03	0.61 ± 0.03	0.54 ± 0.02	0.61 ± 0.06	0.63 ± 0.02	0.66 ± 0.04	0.60 ± 0.05	0.67 ± 0.05
Al ₂ O ₃	17.52 ± 0.07	17.89 ± 0.44	14.70 ± 0.15	18.31 ± 0.06	18.07 ± 1.02	17.58 ± 0.04	18.14 ± 0.15	18.47 ± 0.53	17.66 ± 0.13
FeO	2.78 ± 0.05	2.81 ± 0.06	2.99 ± 0.05	2.30 ± 0.09	2.95 ± 0.48	2.73 ± 0.10	3.87 ± 1.30	2.51 ± 0.11	2.74 ± 0.11
MnO	0.33 ± 0.02	0.37 ± 0.01	0.09 ± 0.03	0.18 ± 0.04	0.35 ± 0.16	0.31 ± 0.07	0.20 ± 0.09	0.24 ± 0.02	0.31 ± 0.06
MgO	0.33 ± 0.03	0.34 ± 0.02	0.62 ± 0.03	0.41 ± 0.02	0.40 ± 0.02	0.36 ± 0.01	1.18 ± 0.66	0.45 ± 0.00	0.35 ± 0.02
CaO	1.02 ± 0.03	1.07 ± 0.07	2.19 ± 0.09	1.37 ± 0.02	1.17 ± 0.22	1.05 ± 0.04	3.55 ± 1.99	1.28 ± 0.10	1.09 ± 0.02
Na ₂ O	8.58 ± 0.05	6.71 ± 2.51	4.21 ± 0.04	6.93 ± 0.08	6.75 ± 2.77	8.49 ± 0.15	5.65 ± 1.28	5.20 ± 2.90	8.32 ± 0.09
K ₂ O	6.05 ± 0.03	5.91 ± 0.03	4.71 ± 0.04	7.26 ± 0.04	6.28 ± 0.35	5.94 ± 0.12	6.72 ± 0.15	6.48 ± 0.29	6.05 ± 0.01
P ₂ O ₅	0.08 ± 0.02	0.05 ± 0.03	0.14 ± 0.01	0.08 ± 0.03	0.03 ± 0.03	0.04 ± 0.03	0.25 ± 0.16	0.08 ± 0.03	0.06 ± 0.02
SO ₂	0.04 ± 0.02	0.04 ± 0.04	0.00 ± 0.00	0.12 ± 0.02	0.04 ± 0.07	0.03 ± 0.02	0.24 ± 0.16	0.06 ± 0.00	0.04 ± 0.02
Cl	0.49 ± 0.01	0.61 ± 0.03	0.16 ± 0.01	0.27 ± 0.02	0.49 ± 0.22	0.52 ± 0.00	0.33 ± 0.03	0.35 ± 0.08	0.52 ± 0.02
F	0.30 ± 0.02	0.35 ± 0.04	0.10 ± 0.03	0.14 ± 0.02	0.31 ± 0.11	0.31 ± 0.01	0.14 ± 0.06	0.20 ± 0.01	0.31 ± 0.04
Total:	96.67 ± 0.36	92.97 ± 0.83	94.26 ± 0.52	94.63 ± 0.13	94.01 ± 0.86	96.18 ± 1.08	95.69 ± 1.65	93.13 ± 2.27	95.61 ± 1.02

Table 4 (continued).

Core, section:	2H-1	2H-1	2H-1	2H-1	2H-1	2H-1	2H-1	2H-1
Interval:	37–38 cm	37–38 cm	37–38 cm					
Sample:	7601-20	7601-21	7601-23	7601-24	7601-26	7601-27	7601-4	7601-25
N:	3	3	3	3	3	3	1	1
SiO ₂	62.38 ± 0.08	60.14 ± 0.28	57.17 ± 0.17	61.94 ± 0.02	62.24 ± 0.08	61.96 ± 0.12	62.98	62.38
TiO ₂	0.48 ± 0.02	0.57 ± 0.02	0.69 ± 0.01	0.50 ± 0.04	0.62 ± 0.02	0.61 ± 0.04	0.60	0.40
Al ₂ O ₃	18.49 ± 0.06	18.20 ± 0.13	18.29 ± 0.11	18.55 ± 0.13	18.14 ± 0.08	17.64 ± 0.10	18.32	18.17
FeO	2.28 ± 0.11	3.36 ± 0.05	4.77 ± 0.19	2.32 ± 0.09	2.47 ± 0.04	2.81 ± 0.18	2.71	2.31
MnO	0.14 ± 0.04	0.12 ± 0.03	0.15 ± 0.03	0.14 ± 0.04	0.24 ± 0.05	0.35 ± 0.03	0.40	0.13
MgO	0.33 ± 0.03	0.93 ± 0.06	1.58 ± 0.07	0.42 ± 0.02	0.40 ± 0.03	0.33 ± 0.01	0.30	0.34
CaO	1.82 ± 0.02	3.14 ± 0.10	4.84 ± 0.08	1.91 ± 0.05	1.27 ± 0.01	1.04 ± 0.01	0.55	1.83
Na ₂ O	5.77 ± 0.05	5.48 ± 0.01	4.87 ± 0.01	5.66 ± 0.04	7.14 ± 0.07	8.31 ± 0.13	7.00	5.95
K ₂ O	7.54 ± 0.19	7.21 ± 0.08	6.62 ± 0.14	8.10 ± 0.08	6.75 ± 0.05	6.02 ± 0.05	5.89	7.71
P ₂ O ₅	0.09 ± 0.04	0.21 ± 0.04	0.35 ± 0.00	0.07 ± 0.03	0.06 ± 0.02	0.04 ± 0.05	0.02	0.06
SO ₂	0.10 ± 0.07	0.17 ± 0.03	0.27 ± 0.03	0.08 ± 0.04	0.10 ± 0.02	0.03 ± 0.02	0.06	0.14
Cl	0.43 ± 0.03	0.34 ± 0.02	0.32 ± 0.02	0.22 ± 0.01	0.38 ± 0.01	0.57 ± 0.05	0.80	0.45
F	0.15 ± 0.03	0.13 ± 0.01	0.08 ± 0.03	0.09 ± 0.04	0.19 ± 0.01	0.29 ± 0.04	0.35	0.13
Total:	92.98 ± 0.81	94.17 ± 0.18	96.50 ± 0.52	96.11 ± 1.00	93.57 ± 0.18	93.61 ± 1.88	96.54	93.46

icantly higher. The layer is interpreted to represent a reworked fallout ash bed.

Sample tr-7502 (161-974B-11H-7, 4–5 cm)

Layer tr-7502 is a ~5-mm-thick, primary or slightly reworked, fallout ash bed. Its relatively high content of foraminifers is probably a sampling artifact. Glass shards in tr-7502 (~60 vol%) are uniformly colorless to pale brown, poorly vesicular to dense. Major-element compositions of the glass shards are highly evolved, silica undersaturated, trachyphonolitic (shoshonitic), with characteristically high TiO₂ (~0.8 wt%) and FeO (~2.7 wt%) contents (Fig. 3).

Samples vt-7538 (161-974B-9H-6, 99–100 cm) and vt-7539 (161-974B-9H-6, 120–121 cm)

These two samples are from the basal part of a single, 112-cm-thick ash turbidite (9H-6, 33–145 cm). The glass fraction (~90 vol%) consists nearly exclusively of colorless, angular, platy bubble-wall shards (Fig. 2). Rare (<1%) pale brownish, dense to vesicle-poor glass particles are rounded and are interpreted to represent older xenolithic obsidian shards. Euhedral to subhedral crystals (<1–5 vol%) are composed of quartz, plagioclase, K-feldspar, clinopyroxene, and amphibole. Both layers contain significant amounts of foraminifer shells (5–15 vol%). Zeolite mineral aggregates occur only in vt-7539.

The major-element composition of glass shards is high-K rhyolite. Both samples show bimodal compositions, however, and comprise roughly equal proportions of (a) high-K calcalkaline glass shards (HKCA), and (b) glass shards with higher K₂O and Al₂O₃ and lower SiO₂ contents, transitional to shoshonitic high-K calcalkaline magma compositions (HKSH) (Fig. 4).

Samples tr-7545 (161-974B-7H-6, 20–22 cm) and tr-7546 (161-974B-7H-6, 43–45 cm)

Samples tr-7545 and tr-7546 are from top and center of a 60-cm-thick, fine-grained, massive vitric tuff (161-974B-7H-6, 10–70 cm). Glass shards (>99 vol%) consist of colorless, bubble-wall shards, and highly vesicular pumice shards with subspherical and strongly elongated “tubular” vesicles. Quartz and K-feldspar are accessory components (<1 vol%). The glass population comprises shoshonitic trachyte and rhyolite compositions (Figs. 3, 4).

Sample vt-7505 (161-974B-7H-3, 82–84 cm)

Sample vt-7505 represents a slightly reworked fallout ash layer or a thin (5 cm) volcaniclastic turbidite. The glass particle population is

very homogeneous and consists nearly exclusively of colorless, silicic, platy and tricuspat, bubble-wall shards (98 vol%), minor amounts of euhedral crystals (<2 vol%; K-feldspar, plagioclase, and clinopyroxene), and <1 vol% lithic fragments and foraminifer shells (Fig. 2). Major-element compositions are exclusively rhyolitic, but are bimodal. The main component is shoshonitic rhyolite. A minor, second population of glass shards has transitional high-K calcalkaline rhyolitic compositions.

Sample tr-7509 (161-974B-4H-6, 6–7 cm)

Fallout tephra layer tr-7509 is primary or slightly reworked, 2 cm thick, and contains abundant (10 vol%), perfectly euhedral crystals of sanidine, plagioclase, biotite, and clinopyroxene, <1 vol% lithic fragments, and <5 vol% foraminifer shells. Over 85 vol% zeolite aggregates in the size fractions 63–250 µm were analyzed. Relict bubble-wall shards are <1 vol%.

Sample vt-7508 (161-974B-4H-2, 132–134 cm)

This thin, volcaniclastic turbidite or slumped fallout ash layer is 5 cm thick and consists predominantly of zeolite mineral aggregates, 10 vol% euhedral crystals (quartz, biotite, clinopyroxene, amphibole, and titanomagnetite), <5 vol% colorless bubble-wall glass shards, <5 vol% lithics, and <1 vol% foraminifer shells.

Samples vt-7512 (161-974B-3H-4, 49–50 cm), vt-7583 (161-974B-3H-4, 35–36 cm), vt-7572 (161-974B-3H-4, 33–34 cm)

Samples vt-7512 (161-974B-3H-4, 49–50 cm), vt-7583 (161-974B-3H-4, 35–36 cm), and vt-7572 (161-974B-3H-4, 33–34 cm) are three samples from one 35-cm-thick, crudely layered, volcaniclastic turbidite deposit (vitric ash layer; fig. 5, Shipboard Scientific Party, 1996). Sample vt-7512 is from the base, and samples vt-7583 and vt-7572 are from the central part of the deposit. The three samples are similar in their principal composition, with 95–98 vol% glass shards, <1 vol% crystals (quartz ± plagioclase, amphibole, and biotite) and volcanic lithic clasts (vt-7512), and 2–5 vol% foraminifer shells. Glass particle morphologies (Fig. 2) and major-element compositions (Figs. 3, 4), however, are strikingly different.

Sample vt-7512 (161-974B-3H-4, 49–50 cm)

Sample vt-7512 (161-974B-3H-4, 49–50 cm) shows a strongly bimodal composition, both with respect to glass shard types and compositions. It consists predominantly of colorless, platy and cuspat, bubble-wall shards (~60 vol%), and pale brown, vesicle-poor to

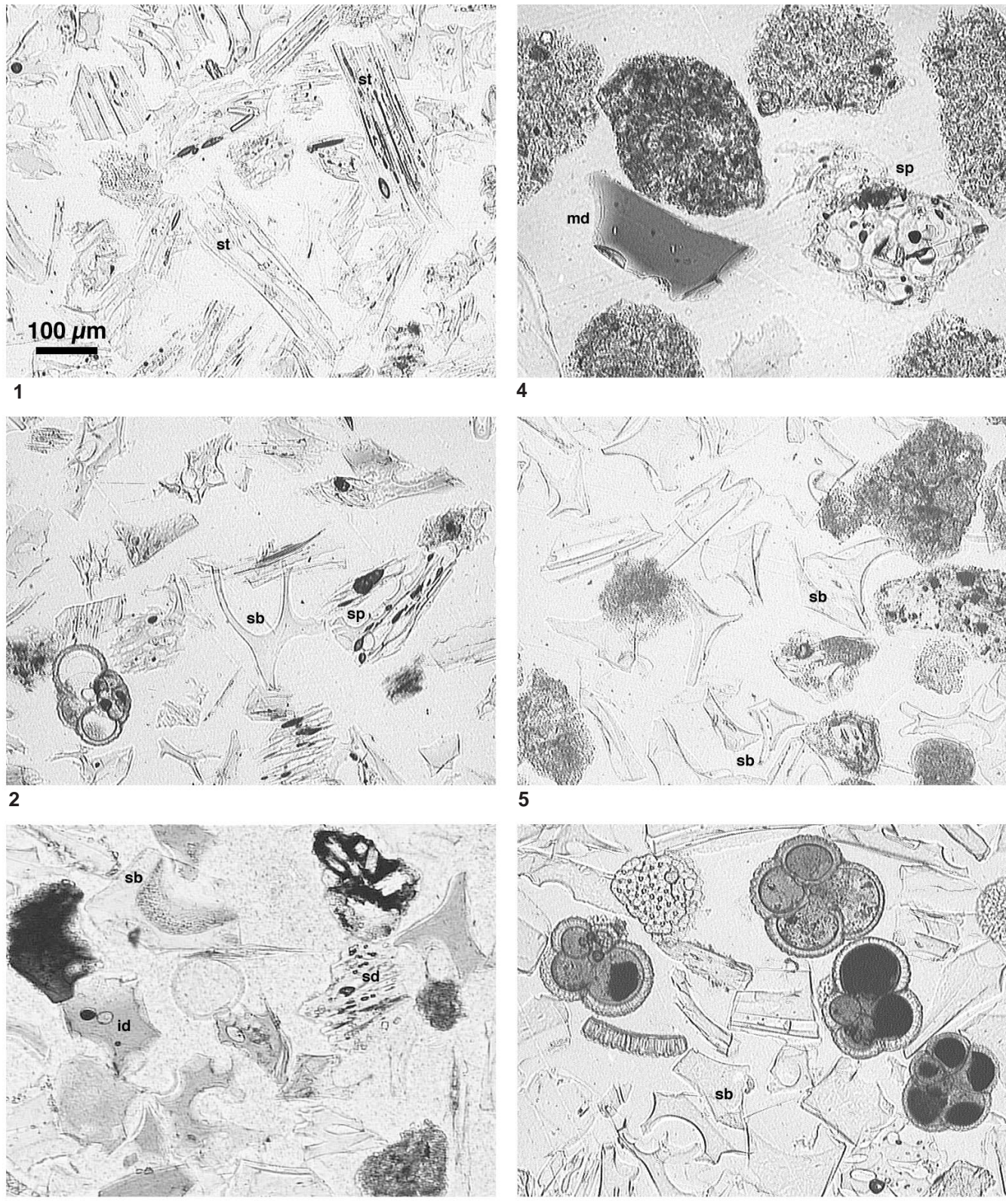


Figure 2. Characteristic glass shard populations from volcanoclastic turbidite samples 7572 (1), 7583 (2), 7512 (3), tephra layers 7600 (4), and 7505 (5), and volcanoclastic turbidite 7538 (6) in thin section. Marked glass shards are silicic tubular pumice (st), silicic, intermediate, and mafic, dense to vesicle-poor shards (sd, id, md), silicic pumice shards (sp) and silicic bubble-wall shards (sb).

dense, bubble-wall and pumice shards (~40 vol%), with bubble-wall thicknesses typically in the 20–50 µm range. Moderately vesicular, colorless pumice shards occur as accessory components. Chemically, the colorless glass shards represent high-K calc-alkaline and shoshonitic rhyolite magma compositions, whereas the pale brown glass shards have high-K calc-alkaline andesitic to trachyandesitic compositions.

Sample vt-7583 (161-974B-3H-4, 35–36 cm)

Sample vt-7583 (161-974B-3H-4, 35–36 cm) comprises two glass shard populations as well. Colorless, platy, and tricuspathe bubble-wall shards and vesicular pumice shards with slightly elongated “tubular” vesicles are the main component (Type A: ~95 vol%; bubble-wall thicknesses typically 5–10 μm), in addition to more vesicle poor to dense, pale to dark brown glass shards with subspherical bubbles (Type B: ~5 vol%). Major-element compositions range from rhyolite (Type A) to dacite and andesite (Type B). All glass shards analyzed from vt-7583 represent members of the low-K calc-alkaline suite of magma compositions.

Sample vt-7572 (161-974B-3H-4, 33–34 cm)

Sample vt-7572 (161-974B-3H-4, 33–34 cm), immediately overlying vt-7583 (161-974B-3H-4, 35–36 cm), consists nearly exclusively of colorless tubular to fibrous pumice shards and bubble-wall shards with extremely elongated vesicles (99 vol%; <1% pale brown, vesicle-poor shards). Chemically, the glass shards are similar to the calc-alkaline rhyolite component of vt-7512. The only glass shard analyzed from this layer shows a high-K calc-alkaline rhyolite composition, but slightly higher K₂O (4.36 wt%) and CaO (2.78 wt%) contents than glass shards from vt-7512 (K₂O ~ 3.5 wt%; CaO ~ 2.4 wt%).

Sample vs-7603 (161-974B-2H-6, 42–43 cm)

This is a 3-cm-thick, well-sorted volcaniclastic crystal-lithic sand layer with >70 vol% crystals (K-feldspar, clinopyroxene, titanite, plagioclase), and ~25% foraminifer shells. Glass particles form <5 vol% of the deposit and consist chiefly of colorless bubble-wall shards, vesicle-poor to dense and tubular pumice shards.

Sample vs-7602 (161-974B-2H-5, 63-63 cm)

This sample is a vitric, crystal- and foraminifer-rich volcaniclastic sand layer (4 cm) with up to 40 vol% glass shards. The highly heterogeneous glass shard population contains approximately equal amounts of both colorless and pale brown pumice shards with subspherical bubbles, platy bubble-wall shards, dense blocky shards, and tubular pumice shards. Its mineral assemblage consists of K-feldspar, clinopyroxene, amphibole, titanomagnetite, and quartz.

Sample vt-7514 (161-974B-2H-5, 30–33 cm)

This sample is from the base of a 37-cm-thick, vitric, crystal- and foraminifer-rich volcaniclastic turbidite deposit. The crystal assemblage (10 vol%) consists of biotite, feldspar, and quartz. Glass shards (20 vol%) are predominantly colorless, platy bubble-wall shards, apart from minor pumice shards (<5 vol%).

Sample vs-7513 (161-974B-2H-4, 35–38 cm)

The crystal-rich, volcaniclastic sand layer vs-7513 represents a sample from the upper part of a 150-cm-thick, volcaniclastic turbidite

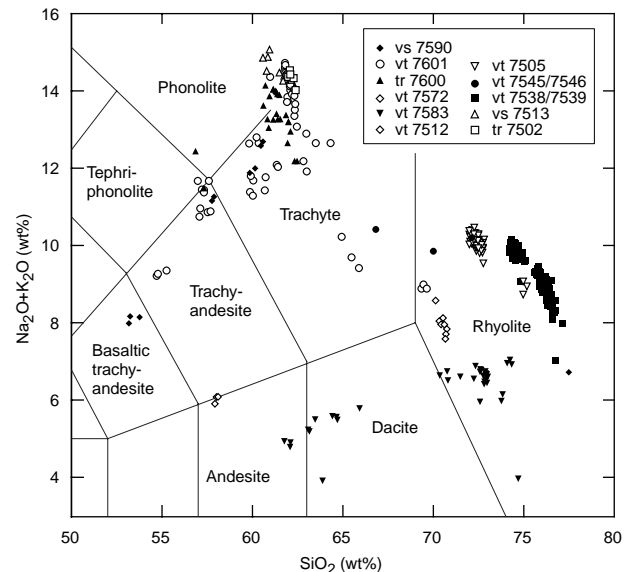


Figure 3. Section of the total alkali-silica diagram (TAS) showing the composition of glass shards from tephra layers and volcaniclastic deposits at Site 974 (electron microprobe data). TAS diagram classification according to Le Maitre et al. (1989).

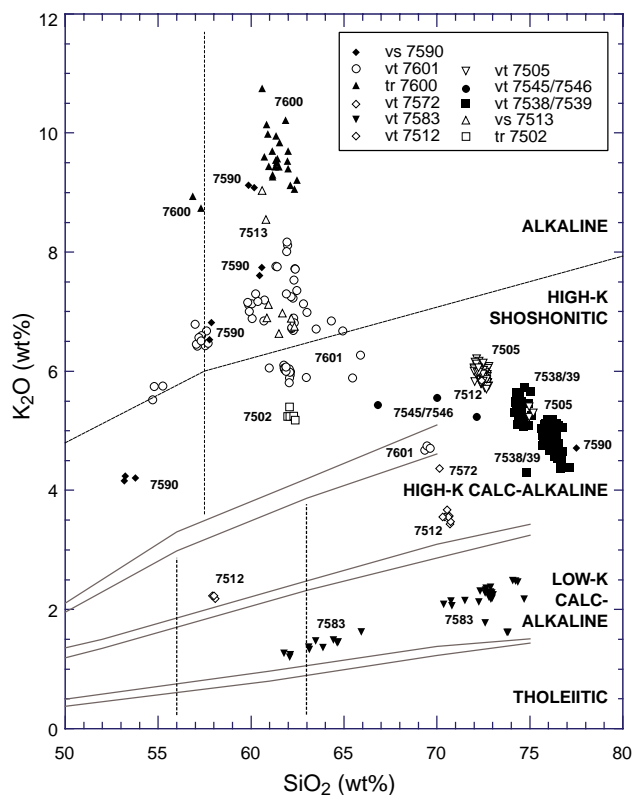


Figure 4. SiO_2 vs. K_2O variation diagram depicting the compositional ranges of glass shards and magma suites represented by tephra layers (tr), volcanoclastic turbidites (vt), and volcaniclastic crystal-lithic sand layers (vs) from Hole 974B. Field boundaries are from Rickwood (1989).

sequence, comprising the entire Section 4 of Core 161-974B-2H. Subhedral crystals (75 vol%; K-feldspar, clinopyroxene, amphibole, plagioclase), volcanic lithic clasts (10 vol%) and foraminifer shells are the main components. Volcanic glass shards (~5 vol%) comprise colorless to pale olive-brown, bubble-wall and dense shards. The glass shards have alkaline magma compositions. Both phonolitic and trachytic compositions (Le Maitre et al., 1989) are present (Figs. 3, 4).

Sample tr-7600 (161-974B-2H-3, 22–23 cm)

This is a 3-cm-thick, well-sorted, primary or slightly reworked, vitric fallout ash bed, consisting of 98 vol% of glass shards, ~2 vol% euhedral crystals (K-feldspar, amphibole, plagioclase, clinopyroxene, and biotite), and <1% altered volcanic lithic clasts (Fig. 2). The glass shard population is dominated by colorless microvesicular pumice and tubular pumice shards (95 vol%). Pale to dark brown, vesicle-poor to dense blocky shards form ~5% of the glass fraction. The chemical compositions of the glass shards are highly alkaline (up to 10 wt% K_2O and 4.5 wt% Na_2O), chiefly phonolitic-trachytic; the more mafic glass shards represent tephriphonolites/trachyandesites (Figs. 3, 4).

Sample vt-7601 (161-974B-2H-1, 37–38 cm)

Sample 7601 represents the top of a 4-cm-thick, vitric volcanoclastic turbidite layer consisting mainly of glass shards (~95 vol%), foraminifer shells (~5 vol%), and accessory subhedral crystals (i.e., K-feldspar, amphibole, and clinopyroxene). Glass particles comprise colorless to dark brown, platy bubble-wall shards and vesicle-poor to dense blocky shards. Chemical compositions of glass shards are highly diverse and reflect dominantly alkaline (phonolitic and trachytic to trachyandesitic), but also shoshonitic (trachytic), and transitional high-K calc-alkaline (rhyolitic) magma compositions.

Samples vs-7588 (161-974B-1H-5, 28–29 cm) and vs-7591 (161-974B-1H-4, 17–18 cm)

These 8-mm- (7588) and 2-cm- (7591) thick, ash-bearing layers represent vitric, foraminiferous volcanoclastic sands composed of ~40 vol% glass shards, 30–40 vol% foraminifer shells, and 10–15 vol% of crystals (K-feldspar, biotite, amphibole ± quartz, and clinopyroxene), and altered volcanic lithics. Glass particles are dominantly colorless bubble-wall shards, pumice shards, and tubular pumice. In addition, sample vs-7588 contains <5 vol% angular, dense, brown glass shards.

Sample vs-7590 (161-974B-1H-3, 57–58 cm)

Sample vs-7590 is from the base of a 12-cm-thick, foraminiferous crystal-lithic volcanoclastic sand or turbidite deposit. With <10 vol% volcanic glass shards (Fig. 2), 60 vol% crystals (K-feldspar, plagioclase, quartz, clinopyroxene, biotite, and titanomagnetite; in part, rounded), 20 vol% foraminifers, and ~10 vol% rounded volcanic lithics, this deposit exhibits the most extreme range of magma compositions observed in the volcanoclastic deposits from Hole 974B. Glass shards range from colorless pumice, to pale brown vesicle-poor, to dark brown, dense, and blocky particles, and chemical compositions range from silica undersaturated, to alkaline trachyte (similar to high-K trachytes in tr-7600 and vs-7513), to trachyandesite (similar to trachyandesites in vs-7601), to basaltic trachyandesite (shoshonite), and to silica-oversaturated high-K calc-alkaline rhyolite (similar to high-silica rhyolite components in vt-7538/7539) (Figs. 3, 4).

Age Determinations

Laser $^{40}\text{Ar}/^{39}\text{Ar}$ age determinations were performed on sanidine and biotite crystals from fallout tephra layer tr-7509 (161-974B-4H-6, 6–7 cm), biotite crystals from volcanoclastic turbidite vt-7508 (161-974B-4H-2, 132–134 cm), volcanoclastic sand layers vs-7500 (161-974B-22X-CC, 30–32 cm), vs-7514 (161-974B-2H-5, 30–33 cm), and vs-7513 (161-974B-2H-4, 35–38 cm) (Tables 5, 6). Individual sanidine crystals were fused and evaporated in a single step (single-crystal analyses). Biotites were analyzed by laser step-heating, without temperature measurements. Heating schedules involved up to 14 steps during which the laser power output was increased from ~40 mW to 2000 mW. Complete degassing of the samples was ensured by a terminal 10-W fusion that yielded mass-39 signals at background level.

Sample tr-7509 (161-974B-4H-6, 6–7 cm)

Eight sanidine crystals, 29 μg –54 μg , were recovered from tr-7509 and analyzed by single-grain fusion. Single-crystal apparent ages range from 476 ± 63 Ka to 616 ± 48 Ka and yield a mean apparent age of 550 ± 20 Ka (mean square weighted deviates [MSWD] = 1.22) (Fig. 5). Regression of $^{36}\text{Ar}/^{40}\text{Ar}$ vs. $^{39}\text{Ar}/^{40}\text{Ar}$ yields a poorly defined isochron with an “age” of 400 ± 500 Ka and an initial $^{40}\text{Ar}/^{36}\text{Ar}$ ratio of 900 ± 2000 (MSWD = 1.05). With regressed ^{36}Ar peak signals ($<4.2 \times 10^{-14} \pm 3.0 \times 10^{-15} \text{ cm}^3 \text{ STP}$ [standard temperature and pressure]) barely above, and sometimes even below, system blank measurements ($3.3 \times 10^{-14} \pm 1.0 \times 10^{-15} \text{ cm}^3 \text{ STP}$), however, the accuracy of the measured $^{36}\text{Ar}/^{40}\text{Ar}$ ratios and corrections for mass discrimination and nonradiogenic “atmospheric” ^{40}Ar ($=^{36}\text{Ar} \times 295.5$) are a serious concern, even if crystals are as radiogenic as the microsanidines from tr-7509.

A single biotite crystal (0.346 mg) from sample tr-7509 was analyzed by laser $^{40}\text{Ar}/^{39}\text{Ar}$ step-heating (12 heating steps; 50 mW–10 W laser power) and yielded a reasonably flat age spectrum with a 77% ^{39}Ar plateau region (Fig. 5). The apparent age calculated from the plateau steps (510 ± 20 Ka) and the integral age (540 ± 30 Ka) of 7509-biotite are identical to the mean apparent age of 7509-sanidine within analytical error limits. Isotope correlation gives an initial $^{40}\text{Ar}/^{36}\text{Ar}$ ratio of 330 ± 20 , and an isochron age of 470 ± 40 Ka (MSWD = 0.79).

Sample vt-7508 (161-974B-4H-2, 132–134 cm)

A single biotite crystal (0.278 mg) from volcanoclastic turbidite vt-7508 was analyzed by laser $^{40}\text{Ar}/^{39}\text{Ar}$ step-heating (17 heating steps; 40 mW–10 W). The resulting age spectrum (Fig. 5) shows plateau regions both in the mid-temperature range (P1: 200–40 mW; 54 vol% ^{39}Ar released), and in the low-temperature range (P2: 100–300 mW; 60 vol% ^{39}Ar released); plateau ages range from 420 ± 40 Ka (P2) to 480 ± 40 Ka (P1). The integrated age (540 ± 40 Ka), isochron age (470 ± 40 Ka) and plateau age 1 appear to be affected by a high- $^{40}\text{Ar}*/^{39}\text{Ar}_K$ component, released chiefly during the high-temperature heating step 12 (500 mW; apparent age = 1.2 ± 0.3 Ma). Therefore, plateau age 2 (420 ± 40 Ka) is considered to give the best age estimate for the final isotopic closure (and eruption) of biotite 7508.

Sample vs-7514 (161-974B-2H-5, 30–33 cm)

A single biotite crystal (0.088 mg) from volcanoclastic sand vs-7514 was dated by laser $^{40}\text{Ar}/^{39}\text{Ar}$ step-heating analysis (14 steps; 40 mW–10 W). Apparent ages of single steps representing releases of $^{39}\text{Ar} > 1$ vol% range from 30 ± 3 Ma to 74 ± 1 Ma. The integrated age is 65.8 ± 0.4 Ma. A contiguous plateau region sensu stricto, with ap-

parent ages overlapping within 1σ error limits and significant (>50%) vol% ^{39}Ar , is not defined, but six heating steps comprising 55 vol% of the total ^{39}Ar released indicate that biotite 7514 cooled below closing temperature at ~ 73 Ma (Fig. 6). Low-temperature, low- $^{40}\text{Ar}^*/^{39}\text{Ar}_K$ heating steps probably reflect argon loss resulting from alteration.

Sample vs-7513 (161-974B-2H-4, 35–38 cm)

A single biotite crystal (0.032 mg) from volcaniclastic sand vs-7513 was analyzed in 12 heating steps (40 mW–10 W) and shows a highly disturbed age spectrum (Fig. 6). Apparent ages of significant heating steps range from 57 ± 1 Ma to 187 ± 1 Ma. The integrated age is determined as 164.9 ± 0.6 Ma.

Sample vs-7500 (161-974B-22X-CC, 30–32 cm)

Sample 7500 (161-974B-22X-CC, 30–32 cm) was taken from the very base of Hole 974B (202.9 mbsf). Petrographic inspection indicated the deposit to represent epiclastic rather than volcaniclastic sand, consisting chiefly of well-rounded quartz crystals and lithics, foraminifer shells, and minor (<5 vol%), subhedral biotite crystals. Volcanic glass shards were not detected in this sample. In Comas, Zahn, Klaus, et al. (1996), Sample 161-974B-22X-CC, 30–32 cm, is not listed among the 207 ash-bearing layers of Hole 974B, but coarse- and fine-grained, dark ash concentrations are reported from Section 161-974C-22X-4 at a similar depth (199.47–199.59 mbsf; Shipboard Scientific Party, 1996).

The 14-step laser $^{40}\text{Ar}/^{39}\text{Ar}$ analysis of a 0.085-mg biotite crystal from sample vs-7500 yields apparent ages around 290 Ma. Six heating steps form a perfect plateau in the age spectrum diagram (Fig. 6), overlap within 1σ error limits and cover 85% of the total ^{39}Ar volume released by the biotite crystal. The plateau age is determined to be 291.2 ± 0.5 Ma, identical to the integrated age (290.3 ± 0.5 Ma), within error limits.

DISCUSSION AND CONCLUSIONS

Ages of Hole 974B Tephra Layers and Volcaniclastic Sediments

The $^{40}\text{Ar}/^{39}\text{Ar}$ laser ages of tephra tr-7509 (510 ± 20 Ka) and volcaniclastic turbidite vt-7508 (420 ± 40 Ka) provide an important time marker in a part of the upper Pleistocene sedimentary sequence at Hole 974B where biostratigraphic ages are scarce (Shipboard Scientific Party, 1996). On the basis of Pliocene to mid-Pleistocene biostratigraphic tiepoints (Shipboard Scientific Party, 1996) and the $^{40}\text{Ar}/^{39}\text{Ar}$ ages of tephras tr-7509 and vt-7508, an age-depth diagram has been constructed that allows a rough estimate to be made of the depositional ages of the volcaniclastic and tephra deposits in Hole 974B (Fig. 7).

Linear interpolation, done exclusively from biostratigraphic age points, indicates approximate depositional (vt, vs) and eruption ages (tr) between 2.95 Ma and 1.25 Ma for volcaniclastic deposits in the upper Pliocene to mid-Pleistocene section (tr-7501, tr-7502, vt-7538/7539, tr-7545/7546, and tr-7505).

Combination of late Pleistocene biostratigraphic tiepoints and $^{40}\text{Ar}/^{39}\text{Ar}$ laser ages of tephras 7509 and 7508 indicates that tephra and volcaniclastic deposits from the upper Pleistocene sequence were erupted and/or deposited between 0.32 Ma (vt-7512) and 0.05 Ma (vs-7590). Average sedimentation rates (uncorrected for compaction) increase from 27 m/m.y. in the late Pliocene (Shipboard Scientific Party, 1996) to 37 m/m.y. during the early and mid-Pleistocene, and nearly double to >66 m/m.y. in the late Pleistocene to Holocene, after the deposition of tr-7509/vt7508 (Fig. 7). Late Pleistocene sedimentation rates exceed the high rates observed after the reestablishment of open-marine conditions in the early Pliocene (52 m/m.y.; Shipboard Scientific Party, 1996).

The increase in the sedimentation rate appears not to be linked directly to the rate of production and influx of volcaniclastic material, as the average number and cumulative thickness of ash deposits (uncorrected for nonvolcanic components) do not differ drastically between the upper Pliocene/lower Pleistocene and the upper Pleistocene cores (Fig. 7). Peak values of 240-cm cumulative thickness between 6.5 and 16 mbsf (~0.1–0.25 Ma) result from the emplacement of a single, exceptionally thick, volcaniclastic turbidite (vs-7513: 150 cm thick). With sedimentation rates >10 \times higher than at Site 974, a significant change in the sedimentary record and increase in sedimentation rate in the mid- to late Pleistocene has been reported from the southeast Tyrrhenian Marsili Basin (Leg 107, Site 650) as well. It is interpreted to reflect the onset of glacial/interglacial climatic fluctuations and eustatic sea-level changes, causing an increase in erosional processes and the efficiency of transport of sediment material into the basin by turbidity currents (Hieke, et al., 1990; Kastens, Mascle, et al., 1990; Muller, 1990; Rio, et al., 1990).

Ages obtained by $^{40}\text{Ar}/^{39}\text{Ar}$ dating from biotite crystals in crystallitic, volcaniclastic sand layers 7514, 7513, and 7500 are in gross disagreement with the depositional ages inferred from biostratigraphic evidence and $^{40}\text{Ar}/^{39}\text{Ar}$ dating of tephras 7509/7508. These biotite crystals range in age from 74 Ma (vs-7514) to 291 Ma (vs-7500) and are interpreted as detritic “epiclastic” components in the volcaniclastic deposits, derived from the erosion of pre-alpine magmatic and metamorphic rocks. A convenient possible source for the sedimentary basin at Site 974 is, for example, Hercynian granitoids on neighboring Sardinia and Corsica, which range in age from 280 Ma to 315 Ma (Sartori, et al., 1987).

Sources and Origin of Hole 974B Tephra Layers and Volcaniclastic Deposits

Pliocene–Pleistocene fallout tephra layers and volcaniclastic deposits in the Tyrrhenian Sea are derived from explosive volcanic

Table 5. Laser $^{40}\text{Ar}/^{39}\text{Ar}$ analyses (sanidine single-crystal data).

Sample description	J-Value	Error 1 σ	No.	Mass (mg)	Apparent age (Ma)	Error 1 σ (Ma)	$^{40}\text{Ar}^*/^{39}\text{Ar}_K$ ($\times 10^{-10}$ cm 3 STP)	Volume cm 3 STP/ mg	Volume $^{39}\text{Ar}_K$ ($\times 10^{-10}$)	Volume $^{40}\text{Ar}_{\text{latm}}$
974B-4H-6, 6–7 cm	9.124E-4	1.0E-6	1	0.054	0.60	0.05	0.37	0.22	4.07	15.69
Sanidine 7509A			2	0.029	0.62	0.05	0.37	0.18	6.29	-3.82
Single crystal fusion			3	0.039	0.49	0.04	0.30	0.25	6.39	15.69
Mean apparent age: 550 ± 20 Ka			4	0.047	0.48	0.06	0.29	0.25	5.39	26.41
Isochron age: 400 ± 500 Ka			5	0.033	0.60	0.08	0.36	0.24	7.22	-5.92
Initial $^{40}\text{Ar}/^{36}\text{Ar}$: 1000 ± 2000			6	0.045	0.55	0.05	0.33	0.31	6.80	7.29
			7	0.041	0.59	0.08	0.36	0.21	5.10	3.54
			8	0.038	0.56	0.08	0.34	0.23	6.12	4.89

Table 6. Laser $^{40}\text{Ar}/^{39}\text{Ar}$ analyses (biotite step-heating data).

Sample	J-value	Error 1 σ	Step	Laser output (mW)	Apparent age (Ma)	Error 1 σ (Ma)	$^{40}\text{Ar}^*/^{39}\text{Ar}_\text{K}$	Volume $^{39}\text{Ar}_\text{K}$ ($\times 10^{-13}$ cm 3 STP)	Volume $^{39}\text{Ar}_\text{K}$ (% cum)	Volume $^{40}\text{Ar}_\text{atm}$ (%)
974B-4H-6, 6-7 cm	9.124E-4	1.0E-6	1	40	-6.01	34.41	-3.64	0.43	0.03	102.18
Biotite 7509B2			2	70	2.47	5.68	1.50	1.43	0.13	93.79
Mass: 0.346 mg			3	100	2.52	1.46	1.53	7.60	0.65	85.62
Step-heating analysis			4	125	0.77	0.47	0.47	14.77	1.66	77.35
Integrated age: 540 \pm 30 Ka			5	150	0.97	0.35	0.59	24.15	3.32	56.43
Isochron age: 470 \pm 40 Ka			6	175	0.84	0.16	0.51	42.86	6.26	43.25
Plateau age: 510 \pm 20 Ka			7	200	0.65	0.15	0.39	72.52	11.23	53.50
			8	250	0.58	0.04	0.35	156.60	21.97	44.40
			9	300	0.55	0.04	0.33	233.92	38.01	41.00
			10	350	0.53	0.07	0.32	139.41	47.57	35.21
			11	400	0.54	0.08	0.33	138.58	57.07	33.87
			12	500	0.46	0.03	0.28	348.50	80.97	52.37
			13	1000	0.50	0.05	0.30	267.30	99.30	44.45
			14	2000	0.95	1.35	0.58	9.92	99.98	-2.84
			15	3000	14.68	74.17	8.96	0.15	99.99	-133.52
			16	5000	-200.20	411.04	-115.12	0.04	100.00	420.33
			17	10000	-325.29	293.85	-180.83	0.06	100.00	308.96
974B-4H-2, 132-134 cm	9.181E-4	9.7E-7	1	40	-0.88	6.69	-0.53	1.49	0.13	101.27
Biotite 7508B2			2	70	-0.09	0.83	-0.06	13.42	1.28	102.55
Mass: 0.278 mg			3	100	0.38	0.28	0.23	40.11	4.73	78.24
Step-heating analysis			4	125	0.39	0.20	0.24	55.05	9.47	65.55
Integrated age: 540 \pm 40 Ka			5	150	0.54	0.14	0.32	49.91	13.77	51.71
Isochron age: 470 \pm 40 Ka			6	175	0.42	0.10	0.25	108.05	23.06	63.40
Plateau age: 420 \pm 40 Ka			7	200	0.33	0.09	0.20	109.58	32.49	71.18
			8	250	0.43	0.04	0.26	166.35	46.80	52.18
			9	300	0.44	0.05	0.26	171.43	61.55	46.84
			10	350	0.51	0.06	0.31	243.23	82.48	50.07
			11	400	0.66	0.28	0.40	47.62	86.58	-27.14
			12	500	1.20	0.27	0.72	39.02	89.94	-70.82
			13	1000	0.52	0.09	0.31	114.39	99.78	3.11
			14	2000	6.62	5.09	4.01	2.44	99.99	-1340.01
			15	3000	759.45	998.15	570.13	0.02	99.99	-2679.91
			16	5000	349.53	354.31	232.86	0.05	100.00	-583.65
			17	10000	423.66	409.17	288.31	0.04	100.00	-38.66
974B-22X-CC, 30-32 cm	9.181E-4	9.7E-7	1	40	159.8	35.8	100.88	0.42	0.13	89.19
Biotite 7500D3			2	70	255.0	4.6	165.40	3.06	1.04	28.00
Mass: 0.085 mg			3	100	286.4	1.2	187.40	35.65	11.68	12.97
Step-heating analysis			4	125	290.9	1.0	190.56	31.04	20.95	6.86
Integrated age: 290.3 \pm 0.5 Ma			5	150	290.9	1.0	190.61	39.18	32.64	2.74
Plateau age: 291.2 \pm 0.5 Ma			6	175	290.2	0.8	190.07	41.62	45.07	1.50
			7	200	292.1	0.6	191.44	44.19	58.26	1.01
			8	250	290.9	0.9	190.57	86.46	84.07	0.57
			9	300	292.3	0.9	191.56	44.34	97.31	0.37
			10	350	275.8	9.3	179.91	1.99	97.90	-0.43
			11	400	338.0	22.9	224.41	0.70	98.11	-5.99
			12	500	300.6	6.5	197.51	2.34	98.81	-0.36
			13	1000	295.2	5.5	193.67	4.01	100.00	-0.21
			14	10000	133.1	1069.1	83.39	-0.01	100.00	114.79
974B-2H-4, 35-38 cm	9.124E-4	1.0E-6	1	40	64.7	3.8	39.99	4.68	4.46	71.23
Biotite 7513B2			2	60	169.6	1.4	108.06	17.95	21.55	11.67
Mass: 0.032 mg			3	80	186.5	1.1	119.39	21.94	42.45	3.02
Step-heating analysis			4	100	179.9	1.1	114.96	21.06	62.51	3.83
Integrated age: 164.9 \pm 0.6 Ma			5	125	152.7	1.9	96.83	12.48	74.40	12.13
Plateau age: n.a.			6	150	153.6	1.4	97.38	11.44	85.29	11.46
			7	175	161.8	3.0	102.87	5.96	90.97	7.09
			8	200	165.8	6.1	105.49	2.23	93.09	5.13
			9	250	164.9	6.2	104.88	2.28	95.26	4.04
			10	350	171.4	7.5	109.24	2.20	97.36	-0.06
			11	700	172.0	11.1	109.67	1.30	98.60	2.89
			12	10000	56.7	13.7	34.99	1.47	100.00	85.86
974B-2H-5, 30-33 cm	9.124E-4	1.0E-6	1	40	29.7	2.7	18.19	12.85	4.85	93.36
Biotite 7514C3			2	70	48.1	0.8	29.63	30.96	16.55	80.05
Mass: 0.088 mg			3	100	59.8	1.2	36.94	34.62	29.62	69.21
Step-heating analysis			4	125	69.7	1.1	43.20	30.18	41.02	64.29
Integrated age: 65.8 \pm 0.4 Ma			5	150	74.0	1.3	45.86	24.11	50.13	63.43
Plateau age: n.a.			6	175	74.6	1.3	46.25	22.23	58.53	63.06
			7	200	71.8	1.1	44.49	20.34	66.21	63.73
			8	250	72.2	0.8	44.76	37.21	80.27	63.05
			9	300	73.4	0.8	45.52	29.99	91.59	61.37
			10	350	73.3	2.5	45.43	13.17	96.57	60.61
			11	400	66.3	1.9	41.03	6.19	98.90	63.43
			12	500	57.3	4.8	35.37	2.63	99.90	67.21
			13	1000	92.4	34.6	57.63	0.32	100.02	52.31
			14	10000	-215.0	193.9	-123.14	-0.05	100.00	-77.41

Note: n.a. = not applicable.

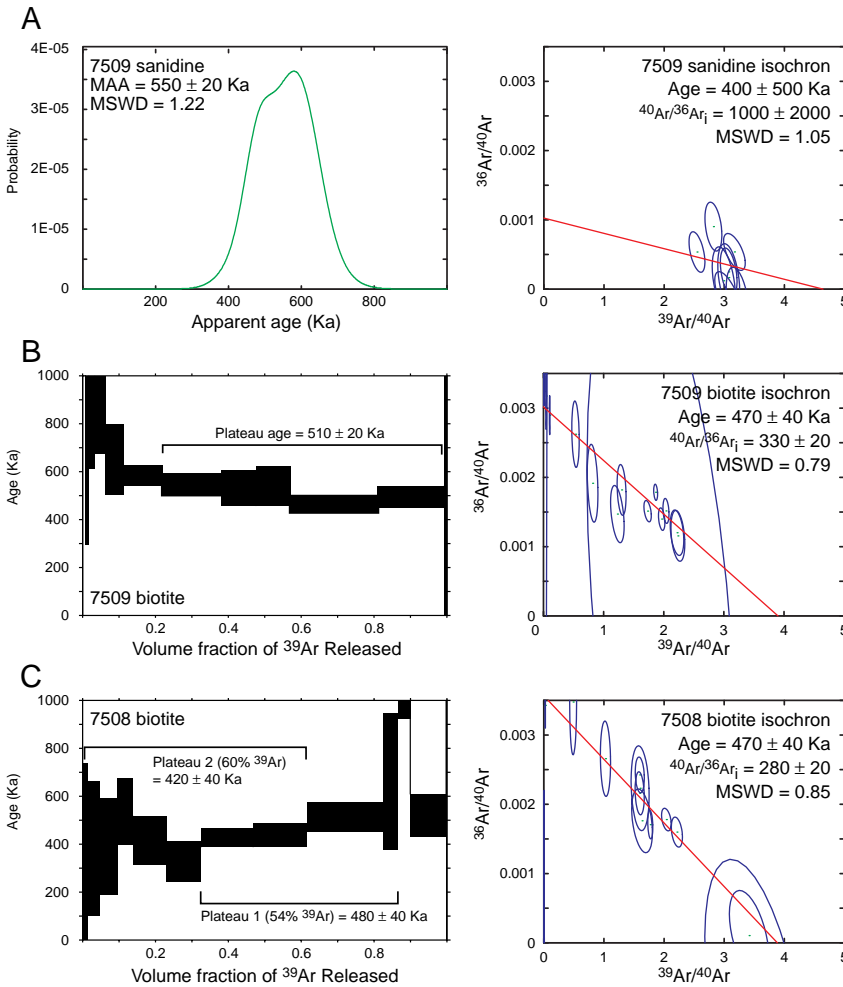


Figure 5. Single-crystal laser $^{40}\text{Ar}/^{39}\text{Ar}$ analyses and laser step-heating analyses from tephra 7509 and volcaniclastic turbidite 7508. **A.** Probability density diagram showing the frequency distribution of apparent ages and isotope correlation diagram of sanidine single-crystal fusions from tr-7509. **B.** Apparent-age spectrum and inverse isochron of laser step-heating analyses of tr-7509 biotite. **C.** Apparent-age spectrum with plateau ranges 1 and 2, and inverse isochron of laser step-heating analyses of tr-7508 biotite. Isotope correlation diagrams show argon isotope composition of individual crystals (sanidine tr-7509) and individual heating steps (biotite tr-7509, and vt-7508) with 1- σ error ellipses. Inverse isochrons determined according to York (1969).

eruptions inside the Tyrrhenian Basin and volcanoes on the Italian mainland (Fig. 1) and from the immediate subaerial to submarine reworking of their pyroclastic deposits (Keller et al., 1978; Paterne et al., 1990; McCoy and Cornell, 1990; Calanchi et al., 1994). Because the different volcanic source areas and magmatic provinces are situated in different tectonic environments, they have developed characteristic magma compositions. Thus, the source of tephra layers and volcaniclastic deposits can be determined by the major-element composition of glass shards and mineral phases in the deposits.

The most important source of Pliocene–Pleistocene tephra deposits in the western Tyrrhenian Sea is a chain of peri-Tyrrhenian volcanic complexes ranging from the older, northwestern Tuscan province (Pliocene; calc-alkaline magmas) to the younger, southeastern Roman Province, which is characterized by potassium-rich, alkaline magma compositions (Beccaluva et al., 1991); the Campanian province is characterized by numerous explosive eruptions of high-K alkaline magmas during the past 200,000 yr (Keller et al., 1978; Keller, 1981; Paterne et al., 1990). Magmas erupted from the Ischia Island subfield have lower $\text{K}_2\text{O}/\text{Na}_2\text{O}$ ratios than those from eruptive centers in the Phleorean fields (Paterne and Guichard, 1993) (Fig. 8). In marine sequences, the Phleorean Fields are represented mainly by trachytic, trachybasaltic, and latictic tephra layers (Paterne, 1985). Phonolitic tephra layers are exposed in the Phleorean Fields and were detected in marine cores (Site 650; McCoy and Cornell, 1990; Calanchi et al., 1994).

The second major source is the Eolian arc, whose volcanic islands and seamounts are characterized by calc-alkaline and shoshonitic magmas and by volcanic activity during most of the Pleistocene until

the present. Calc-alkaline eruptions started earlier (~1.3 Ma) than the shoshonitic compositions (~0.5 Ma) (Barberi et al., 1974; Beccaluva et al., 1981, 1982; Keller, 1982). Low-K calc-alkaline “orogenic” magmas are only known from the Island of Salina (Keller, 1980), but are restricted to mafic magmas.

The Pantelleria peralkaline volcanic complex has been active since 325 Ka (Mahood and Hildreth, 1986) or 220 Ka (Civetta et al., 1984), with several major, in part caldera-forming, explosive eruptions of trachytic to pantelleritic composition, including the eruption of the Green Tuff at 50 Ka (Mahood and Hildreth, 1986). Pleistocene volcanic activity of Mount Etna is characterized by mildly explosive volcanic eruptions of trachybasaltic and trachyandesitic magmas (Keller et al., 1978). Prominent intra-Tyrrhenian, Pliocene–Pleistocene eruptive centers are the seamounts of Vavilov and Magnaghi, which started to erupt alkalic to tholeiitic basalts during the late Pliocene and continued until the Pleistocene (Savelli, 1988), and the Marsili Seamount, which developed in the Pleistocene (<1.7 Ma) and whose magma compositions range from early tholeiitic basalts to calc-alkaline basalt (Beccaluva et al., 1985).

Several of the tephra layers and volcaniclastic turbidites at Site 974 form distinct tephrochronologic marker horizons and can be correlated with specific source areas or even with single eruptions in the Peri-Tyrrhenian volcanic provinces on the basis of their characteristic major-element compositions (Figs. 8, 9) and inferred ages. Ages and compositions of the Site 974 tephra layers and volcaniclastic sediments can also be compared and correlated with the tephrostratigraphic and tephra zones established at the eastern Tyrrhenian Site 650 (Fig. 10; McCoy and Cornell, 1990; Calanchi et al., 1994).

Marker 1

Phonolitic tephra tr-7502 is the oldest volcanic deposit studied from Site 974. Its late Pliocene age (~2.4 Ma) and highly evolved high-K shoshonitic (HKSH) composition ($\text{Na}_2\text{O} \sim 9$ wt%, $\text{TiO}_2 \sim 0.8$ wt%) are unique. Alkali and silica contents (Figs. 8, 9) indicate that the tephra is derived from explosive eruptions in the Tuscan-Roman-Campanian magmatic province. The chemical composition ($\text{Na}_2\text{O} > \text{K}_2\text{O}$, $\text{FeO} \sim 2.7$ wt%) is similar to that of shoshonitic trachytes from the older Campanian Series (i.e., Ponza P39A; 1.1 Ma; Savelli, 1987). The age of the tephra, however, is much greater and corresponds to the older volcanism in the Tuscan province (4.3 to 2.3 Ma) or to earlier eruptions in the Ponza archipelago (up to 4.4 Ma; P13; Savelli, 1987), which are dominantly calc-alkaline rhyolitic-dacitic. Tephra layers with compositions similar to tr-7502 were not detected in sediment cores from the Tyrrhenian basin before Leg 161.

Marker 2

With a consistently bimodal rhyolitic composition, comprising both high-K calc-alkaline glass shards (HKCA) and glass shards transitional to shoshonitic high-K calc-alkaline magma compositions (HKSH), volcaniclastic turbidite vt-7538 represents vitric ash material derived from two different magmas, possibly erupted by two different explosive events, but remobilized and redeposited together in a single turbidite current, without significant addition of vitric components from other eruptions. Major-element compositions of both magma components in vt-samples 7538 and 7539 are nearly identical to rhyolite tephra PLM-2 from Ponza (1.75 Ma; Savelli, 1987), as is the estimated age of the deposit (1.8 Ma; Figs. 9, 10). Older rhyolite magmas erupted from Ponza (P-13; 4.4 Ma; Savelli, 1987) show significantly higher CaO contents (1.16 wt%; Barberi et al., 1967). Volcaniclastic turbidite vt-7538 is, therefore, correlated with the explosive eruption PLM-2 of Ponza (Pontian Islands).

The shoshonitic trachyte and rhyolite glass compositions of vt-7545/7546 are very similar to those of tephra t007 from Site 650 (Figs. 9, 10), correlated to an eruption at Pantelleria at 133 Ka (Calanchi et al., 1994), although this deposit is stratigraphically much older (1.35 Ma) than any of the magmatic phases from Pantelleria (<0.335 Ma; Mahood and Hildreth, 1986).

Marker 3

Tephra 7505 has a characteristic, bimodal, rhyolitic composition, with a dominant shoshonitic rhyolite component, and a minor population of transitional high-K calc-alkaline rhyolite similar to vt-7538. The high-silica shoshonitic composition of its main component is

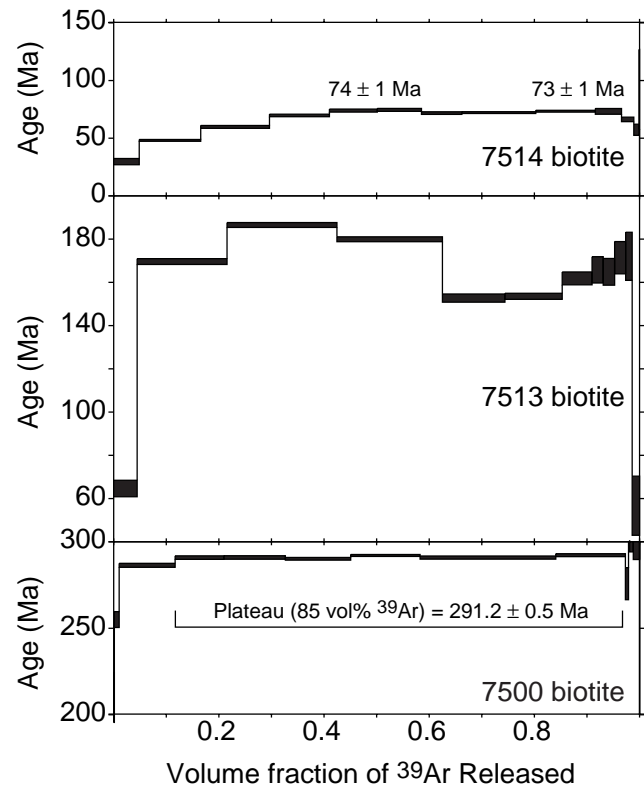


Figure 6. Single-crystal laser step-heating analyses of biotite crystals from volcaniclastic crystal-lithic sand layers vs-7514, vs-7513, and vs-7500. Age spectrum diagrams show apparent ages of individual heating steps with 1σ error bars.

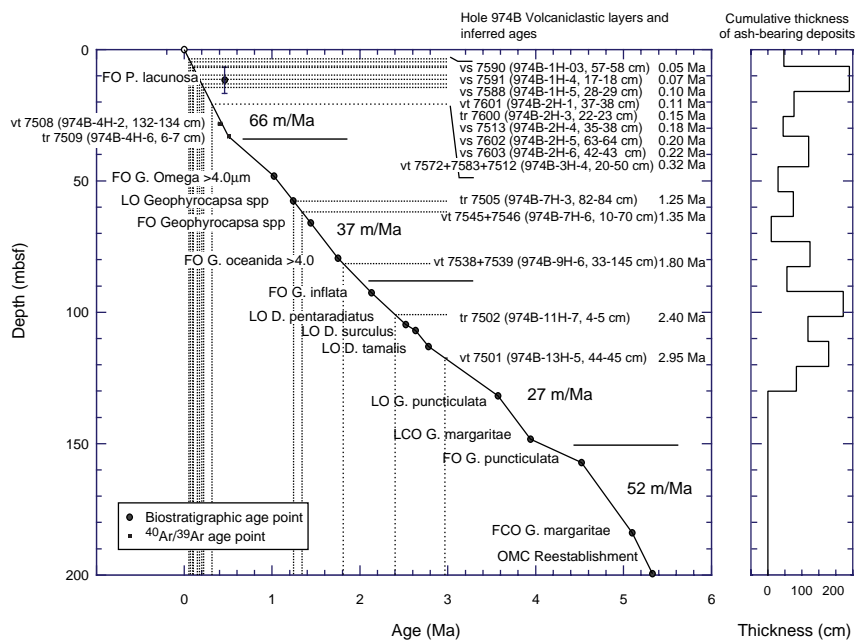


Figure 7. Age vs. depth diagram showing the stratigraphic position and inferred ages of tephra layers and volcaniclastic sediments from Hole 974B (left). Age-depth curve is based on biostratigraphic data points in the 50–200 mbsf depth range (Shipboard Scientific Party, 1996), and the $^{40}\text{Ar}/^{39}\text{Ar}$ ages of tephra layers tr7509 and vt7508 in the 0–50 mbsf depth range (this study). Estimates of Pliocene average sedimentation rates (Shipboard Scientific Party, 1996) and Pleistocene average sedimentation rates (this study) are not corrected for sediment compaction. Note steep increase to >66 m/m.y. in the upper Pleistocene (<0.5 Ma). Right column: Estimate of the variation of the total thickness of ash-bearing deposits in Hole 974B from Cores 1H–22X. Data (from Shipboard Scientific Party, 1996) are not corrected for nonvolcanic components.

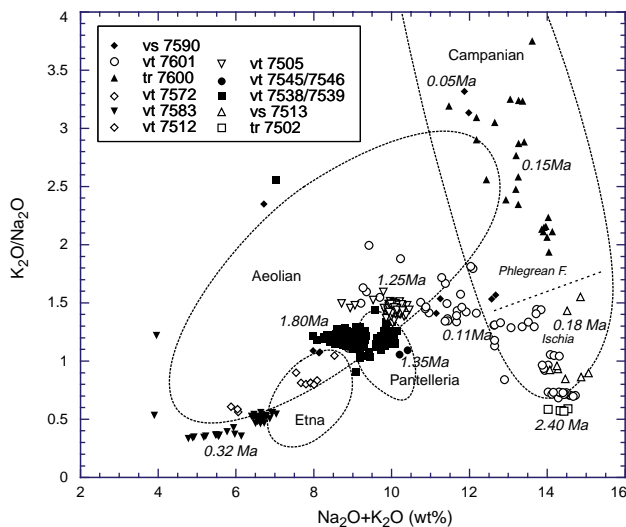


Figure 8. Composition of glass shards from Site 974 tephra layers and volcaniclastic sediments in the $\text{Na}_2\text{O} + \text{K}_2\text{O}$ vs. $\text{K}_2\text{O}/\text{Na}_2\text{O}$ discrimination diagram compared to magma compositions of potential Peri-Tyrrhenian magmatic source provinces. Reference field boundaries of the Campanian, Aeolian, Etna, and Pantelleria volcanic provinces, and Ischia vs. Phleorean fields boundary from various sources, modified from Calanchi et al. (1994). Ponza (Pontine Islands) compositions from Barberi et al. (1967) and Savelli (1987).

unique, and tephra deposits or glass shards in volcaniclastic deposits with similar composition are not known from Leg 107 (McCoy and Cornell, 1990; Calanchi et al., 1994), especially not of this age (1.25 Ma) (Fig. 9). The alkali discrimination diagram indicates either high-K calc-alkaline to shoshonitic eruptions in the Campanian region (Ponza?) or early shoshonitic eruptions in the Eolian arc as possible sources of tephra 7505 (Fig. 8).

Marker 4

Volcaniclastic turbidite vt-7512 (including 7583 and 7572) is the only tephra deposit in the Site 974 sequence so far that contains both high-K calc-alkaline, shoshonitic (poorly constrained), and low-K calc-alkaline magma compositions. Consistent characteristic glass-shard morphologies and abundances, and the available microprobe data, indicate that the turbidity current(s) scavenged tephra material from at least three different explosive eruptions, with no indication of sedimentary mixing of the different populations.

Both vt-7583 and vt-7512 probably represent the products of compositionally zoned eruptions and/or mixed-magma columns, ranging from high-K calc-alkaline trachyandesite to comagmatic rhyolite (7512), from low-K calc-alkaline andesite to comagmatic dacite and rhyolite (7583), respectively.

Rare low-K calc-alkaline rhyolite components have also been reported from three stratigraphic levels at Site 650 (t013, vt036, vt043; Figs. 9, 10) and tentatively attributed to early magmatic stages of the Eolian Island Salina (McCoy and Cornell, 1990; Calanchi et al., 1994), although subaerial exposed low-K calc-alkaline magmas on Salina are restricted to basaltic andesitic compositions (Keller, 1974). Although Site 650 tephra t013 is much older (~0.8 Ma) and major turbidite vt034 is significantly younger (0.13 Ma) than vt-7512, the third volcaniclastic layer vt036 is very similar in age (~0.33 Ma) and glass shard composition to vt-7512 (~0.32 Ma), which may indicate the simultaneous(?) initiation of turbidity currents during and after a series of major explosive eruptions both in the eastern and western Tyrrhenian Basin.

Marker 5

Marker 5 is the advent of K-rich alkaline (ALK) magma compositions in the volcaniclastic sediments of Site 974, related to the late Pleistocene alkaline volcanism in the Roman-Campanian province (i.e., Sabatini, Vulsino, Vico, Phleorean fields, and Ischia). Volcaniclastic crystal-lithic sand vs-7513 is the oldest alkaline-glass-bearing deposit detected in Hole 974B. Alkaline phonolitic and/or trachytic glass shards are thus an omnipresent constituent of volcaniclastic deposits at Site 974 and in the eastern Tyrrhenian sections (McCoy and Cornell, 1990; Calanchi et al., 1994). The inferred age of volcaniclastic sand vs-7513 (0.18 Ma) is slightly younger than the earliest Roman-Campanian alkaline eruptions (~0.2 Ma; Keller, et al., 1978; Paterne et al., 1990), which indicates that some of the volcaniclastic sediments below vs-7513 already belong to the “Campanian stage,” certainly at least vt-7603, whose mineral assemblage includes titanite, but whose glass composition has not yet been analyzed.

Marker 6

Tephra 7600 has a phonolitic-trachytic to tephriphonolitic, alkaline composition typical of magmas erupted from the Phleorean fields. Compositional variation in the deposit probably reflects the eruption from a compositionally zoned, phonolitic-tephritic magma column. Glass compositions are significantly higher in K_2O content than tephras t007, t005, and t003, which are also estimated to be younger (<0.13 Ma; Calanchi et al., 1994) than tr-7600 (~0.15 Ma) (Figs. 8, 9). Tephra 7600 may, however, correlate with a Campanian tephra of equal age (0.15 Ma) reported from Tyrrhenian Core KET 8004 (Paterne et al., 1990).

Nonmarkers

Volcaniclastic, crystal-lithic sand layers vs-7601 and vs-7590 show highly heterogeneous, indistinctive glass populations ranging in composition from alkaline to high-K shoshonitic and high-K calc-alkaline. Individual glass shards range from silica undersaturated, alkaline trachyte (similar to high-K trachytes in tr-7600 and vs-7513), to trachyandesite (similar to trachyandesites in vs-7601) to basaltic trachyandesite (shoshonite), transitional high-K calc-alkaline to shoshonitic rhyolites, and silica-oversaturated high-K calc-alkaline rhyolite (similar to high-silica rhyolite components in vt-7538/7539). Some glass shards in vs-7601 and vs-7590 show compositions very similar to that of (reworked) Campanian Ignimbrite (Keller et al., 1978; Federman and Carey, 1980; Cornell et al., 1983; Paterne et al., 1990), which roughly fits the estimated age of these volcaniclastic deposits (0.05–0.07 Ma). Most of the vitric components in vs-7601 appear to be derived from trachytic eruptions on Ischia (Figs. 8, 9).

Even with a much smaller number of glass-shard analyses (>700 in Calanchi et al., 1994), the volcaniclastic deposits studied from Hole 974B show a wider compositional range of glass and magma compositions compared to those from Leg 107, which probably reflects the dominance of the Eolian Arc as a tephra source in the eastern Tyrrhenian Basins and the proximity of high-K calc-alkaline to shoshonitic older Campanian “Ponza” eruptive centers to Site 974.

Judging from the stratigraphic age range and drill site location (Fig. 1) with respect to postulated prevailing northwesterly paleo-wind directions (Paterne et al., 1990; McCoy, 1981), the Tuscan-Roman-Campanian volcanic provinces, and especially the Pontine Island eruptive centers, were likely to have been the most significant sources of primary fallout tephra layers and volcaniclastic sediment material at Site 974. The occurrence of significant low-K calc-alkaline tephra deposits (vt-7512) >400 km northwest of Salina, the assumed source of mid-Pleistocene low-K calc-alkaline explosive eruptions, however, raises questions about the reliability of general

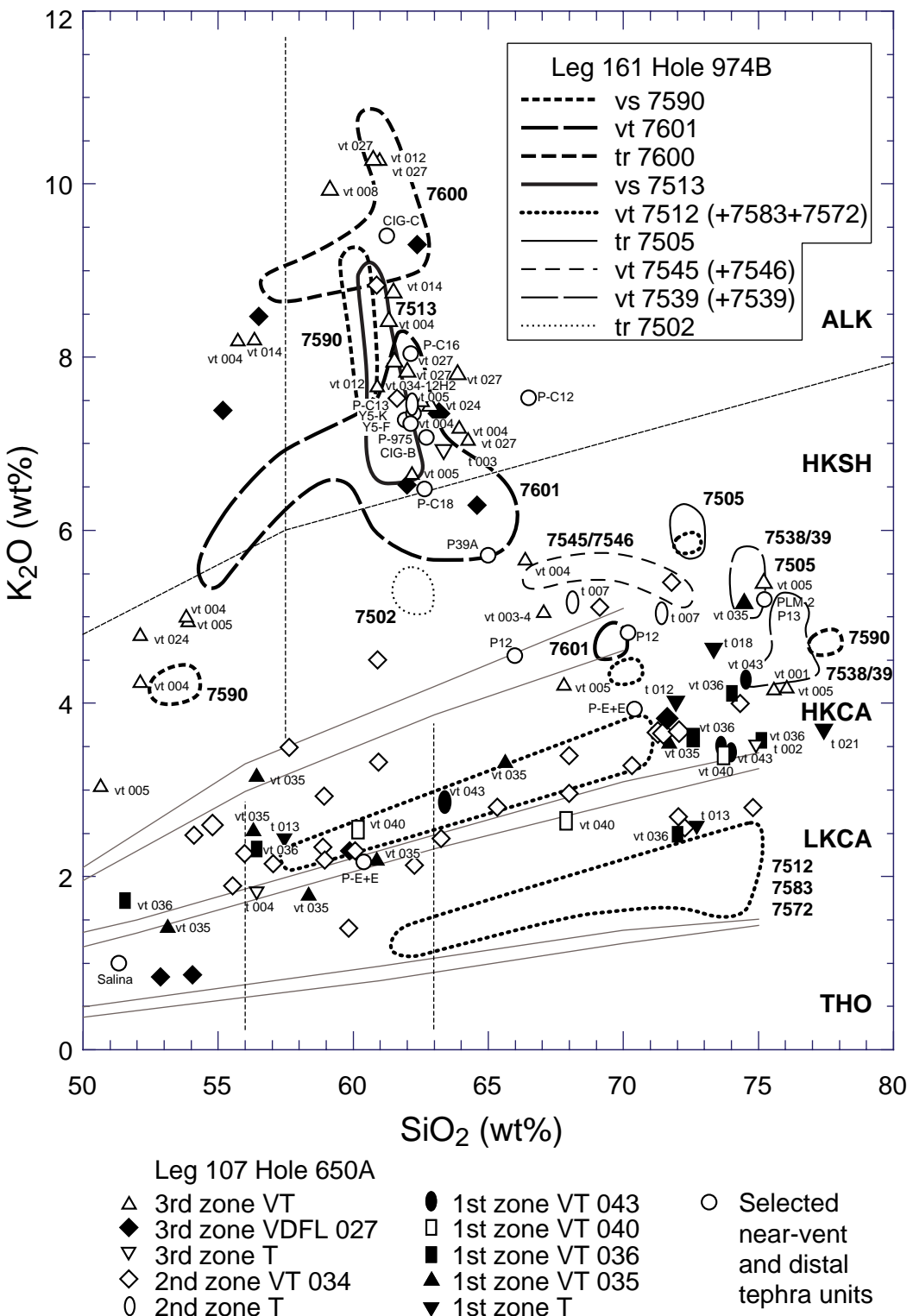


Figure 9. Comparison and correlation of tephra layers and volcaniclastic deposits from central Tyrrhenian Hole 974B (shown with field outlines from electron microprobe (EMP) analyses; Fig. 4) with tephra layers (t), volcaniclastic turbidites (vt), and volcaniclastic density flow deposits (vdfl) in Tephra Zones 1, 2, and 3 from eastern Tyrrhenian Hole 650 (McCoy and Cornell, 1990; Calanchi et al., 1994). Tyrrhenian tephra marker horizons P13, P975, P-C13, P-E + E, and P-C12 from Paterne (1985), Paterne et al. (1986; 1988), Y5 from Keller et al. (1978) and Federman and Carey (1980). Selected near-vent tephra compositions from Cornell et al. (1979) (Campanian Ignimbrite CIG-B and -C), Barberi et al. (1967) (P13; Ponza), and Savelli (1987) (PLM-2 and P39A; Ponza). Symbol sizes reflect single EMP data points (small) and averages of dominant homogeneous glass particle compositions (large). THO = tholeiitic, LKCA = low-K calc-alkaline, HKCA = high-K calc-alkaline, HKSH = high-K shoshonitic, ALK = alkaline. Field boundaries according to Rickwood (1989).

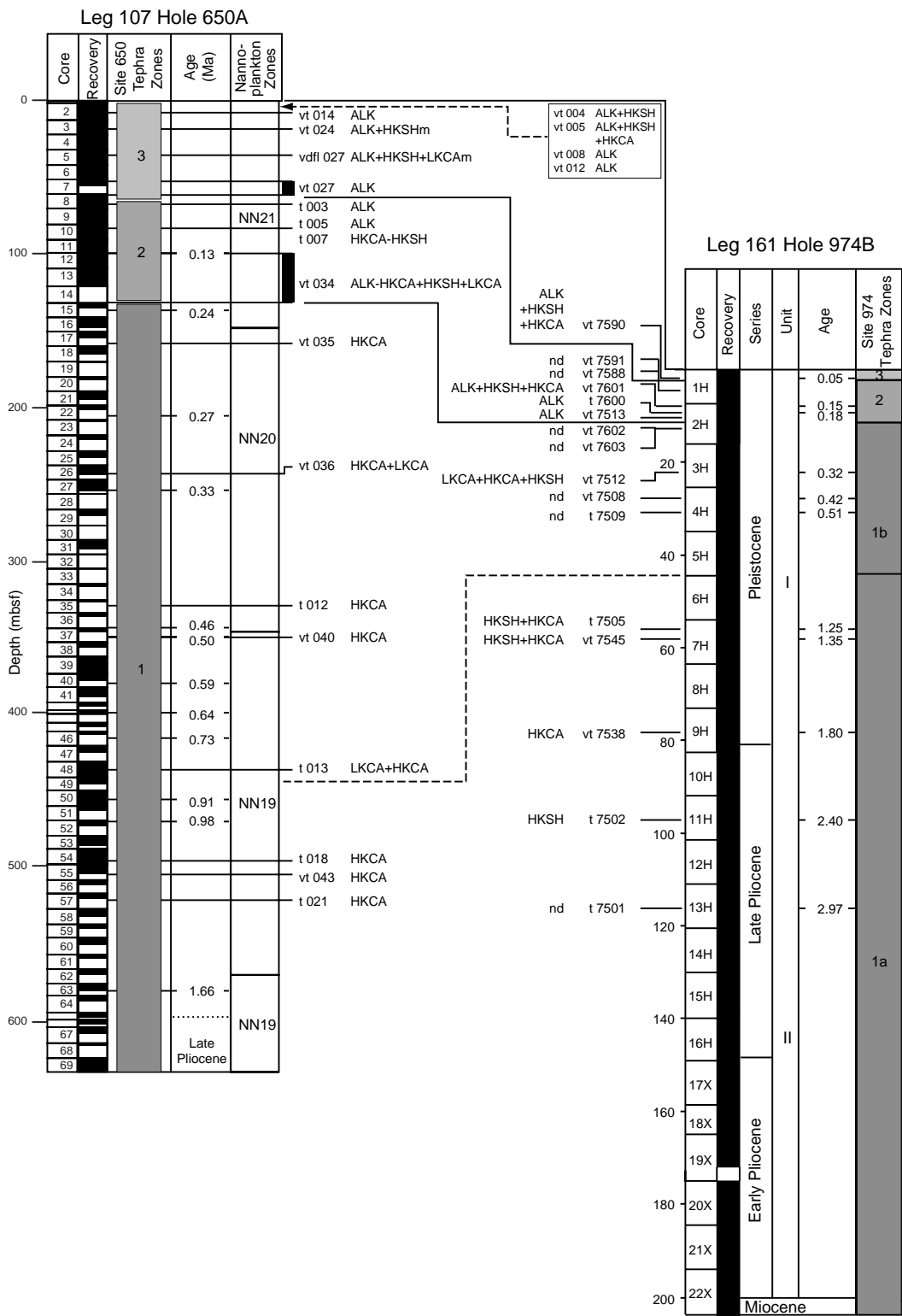


Figure 10. Comparison and correlation of tephra zones, magma compositions, and inferred biostratigraphic and radiometric ages of tephra layers and volcanioclastic deposits in eastern Tyrrhenian Site 650 and central Tyrrhenian Site 974. Core recovery and nannoplankton zones of Site 650 are from Kastens, Mascelle, et al. (1990), of Site 974 are from Shipboard Scientific Party (1996). Biostratigraphic and paleomagnetic ages at Site 650 are from Channell et al. (1990) and Kastens, Mascelle, et al. (1990). Site 650 tephra zones and glass-shard compositions are from Calanchi et al. (1994) and McCoy and Cornell (1990). Note the dominance of high-K calc-alkaline (HKCA) compositions in tephra zones 1a (>3 Ma to 0.8 Ma) and 1b (0.8 Ma to 0.2 Ma), contrasting tephra compositions at eastern Tyrrhenian Site 650 (HKCA + LKCA) and central Tyrrhenian Site 974 (HKCA + LKCA + HKSH) in tephra zones 1a and 1b, and the dominance of alkaline (ALK) magma compositions in tephra zone 2 (0.20 to 0.075 Ma) and tephra zone 3 (0.075 Ma to the present).

northwesterly paleowind directions, or the exclusivity of Salina as a source of mid-Pleistocene, low-K calc-alkaline magmas in the Tyrrhenian backarc system.

Perfect core recovery at Site 974 has provided a detailed, nearly continuous, record of volcanic and volcanoclastic deposits in the western Tyrrhenian Sea. The initial results of this study (with only a fraction of the deposits analyzed and many more to be dated) extend the record of Pliocene–early Pleistocene Tyrrhenian volcanic and magmatic events, which may or may not be preserved in the terrestrial volcanic source areas. Most of the ash layers and many of the volcanoclastic deposits show highly characteristic particle morphologies and major-element fingerprints and thus a high potential for between-core and land-sea correlations.

ACKNOWLEDGMENTS

The authors are grateful to R. Werner and D. Pyle for reviewing the manuscript, P. Gloer for assistance with the microprobe work, J. Sticklus for assistance with argon laser dating, and C. v.d. Bogaard for discussions, critical comments, and suggestions on an early version of the manuscript. This work was supported by the Deutsche Forschungsgemeinschaft (Grant No. Bo 914-6).

REFERENCES

- Barberi, F., Borsi, S., Ferrara, G., and Innocenti, F., 1967. Contributo alla conoscenza vulcanologica e magmatologica delle isole dell' Arcipelago Pontino. *Mem. Soc. Geol. Ital.*, 6:581–606.
- Barberi, F., Civetta, L., Gasparini, P., Innocenti, F., Scandone, R., and Villari, L., 1974. Evolution of a section of the Africa-Europe plate boundary: paleomagnetic and volcanological evidence from Sicily. *Earth. Planet. Sci. Lett.*, 22:123–132.
- Barberi, F., Innocenti, F., Ferrara, G., Keller, J., and Villari, L., 1974. Evolution of Eolian arc volcanism (southern Tyrrhenian Sea). *Earth. Planet. Sci. Lett.*, 21:269–276.
- Beccaluva, L., Di Girolamo, P., and Serri, G., 1991. Petrogenesis and tectonic setting of the Roman Volcanic Province, Italy. *Lithos*, 26:191–221.
- Beccaluva, L., Gabbianelli, G., Lucchini, F., Rossi, P.L., and Savelli, C., 1985. Petrology and K/Ar ages of volcanic dredged from the Eolian seamounts: implications for geodynamic evolution of the southern Tyrrhenian basin. *Earth. Planet. Sci. Lett.*, 74:187–208.
- Beccaluva, L., Gabbianelli, G., Lucchini, F., Rossi, P., Savelli, C., and Zeda, O., 1981. Magmatic character and K/Ar ages of volcanoes dredged from the Eolian seamounts (Tyrrhenian Sea). In Wezel, F. (Ed.), *Sedimentary Basins of Mediterranean Margins*. C.N.R. Ital. Proj. Oceanogr., 361–368.
- Beccaluva, L., Rossi, P.L., and Serri, G., 1982. Neogene to recent volcanism of the southern Tyrrhenian-Sicilian area: implications for the geodynamic evolution of the Calabrian Arc. *Earth Evol. Sci.*, 3:222–238.
- Bitschene, P.R., and Schmincke, H.-U., 1990. Fallout tephra layers: composition and significance. In Heling, D., Rothe, P., Förstner, U., and Stoffers, P. (Eds.), *Sediments and Environmental Geochemistry*. Heidelberg (Springer), 48–82.
- Bogaard, P.V.D., 1995. $^{40}\text{Ar}/^{39}\text{Ar}$ ages of sanidine phenocrysts from Laacher See tephra (12,900 yr BP): chronostratigraphic and petrological significance. *Earth. Planet. Sci. Lett.*, 133:163–174.
- Calanchi, N., Gasparotto, G., and Romagnoli, C., 1994. Glass chemistry in volcanoclastic sediments of ODP leg 107, Site 650, sedimentary sequence: provenance and chronological implications. *J. Volcanol. Geotherm. Res.*, 60:59–85.
- Channell, J.E.T., Rio, D., Sprovieri, R., and Glaçon, G., 1990. Biomagnetostratigraphic correlations from Leg 107 in the Tyrrhenian Sea. In Kastens, K.A., Mascle, J., et al., *Proc. ODP, Sci. Results*, 107: College Station, TX (Ocean Drilling Program), 669–682.
- Civetta, L., Cornette, Y., Crisci, G., Gillot, P.Y., Orsi, G., and Requejo, C.S., 1984. Geology, geochronology and chemical evolution of the island of Pantelleria. *Geol. Mag.*, 121:541–668.
- Comas, M.C., Zahn, R., Klaus, A., et al., *Proc. ODP, Init. Repts.*, 161: College Station, TX (Ocean Drilling Program).
- Cornell, W., Carey, S., and Sigurdsson, H., 1983. Computer simulation of transport and deposition of the Campanian Y-5 ash. *J. Volcanol. Geotherm. Res.*, 17:89–109.
- Cornell, W.C., Sigurdsson, H., and Sparks, R.S.J., 1979. The Campanian Ignimbrite, diversity of glass composition: evidence for a mixed-magma eruption. *Eos*, 60:409.
- Dalrymple, G.B., and Duffield, W.A., 1988. High precision $^{40}\text{Ar}/^{39}\text{Ar}$ dating of Oligocene tephra from the Mogollon-Datil volcanic field using a continuous laser system. *Geophys. Res. Lett.*, 15:463–466.
- Duffield, W.A., and Dalrymple, G.B., 1990. The Taylor Creek Rhyolite of New Mexico: a rapidly emplaced field of lava domes and flows. *Bull. Volcanol.*, 52:475–487.
- Federman, A.N., and Carey, S.N., 1980. Electron microprobe correlation of tephra layers from eastern Mediterranean sediments and the island of Santorini. *Quat. Res.*, 13:160–171.
- Froggatt, P.C., 1992. Standardization of the chemical analysis of tephra deposits: report of the ICCT working group. *Quat. Int.*, 13/14:93–96.
- Hieke, W., Glaçon, G., Hasegawa, S., Müller, C., and Peypouquet, J.P., 1990. Sedimentation in the Marsili Basin during Quaternary (ODP Site 650, Tyrrhenian Sea). In Kastens, K.A., Mascle, J., et al., *Proc. ODP, Sci. Results*, 107: College Station, TX (Ocean Drilling Program), 255–289.
- Hunt, J.B., and Hill, P.G., 1993. Tephra geochemistry: a discussion of some persistent analytical problems. *The Holocene*, 3:271–278.
- Kastens, K.A., Mascle, J., et al., 1990. *Proc. ODP, Sci. Results*, 107: College Station, TX (Ocean Drilling Program).
- Kastens, K.A., Mascle, J., Auroux, C., et al., 1987. *Proc. ODP, Init. Repts.*, 107: College Station, TX (Ocean Drilling Program).
- Keller, J., 1974. Petrology of some volcanic rock series of the Aeolian Arc, southern Tyrrhenian Sea: calc-alkaline and shoshonitic associations. *Contrib. Mineral. Petrol.*, 46:29–47.
- , 1980. The island of Salina. In Villari, L. (Ed.), *The Eolian Islands: An Active Arc in the Mediterranean Sea*. *Rend. Soc. Ital. Mineral. Petrol.*, 36:489–524.
- , 1981. Quaternary tephrochronology in the Mediterranean. In Self, S., and Sparks, R.S.J. (Eds.), *Tephra Studies*. NATO Adv. Study Inst. Ser., 227:244.
- , 1982. Mediterranean island arcs. In Thorpe, R.S. (Ed.), *Andesites*. New York (Wiley), 307–325.
- Keller, J., Ryan, W.B.F., Ninkovich, D., and Altherr, R., 1978. Explosive volcanic activity in the Mediterranean over the past 200,000 yrs as recorded in deep sea sediments. *Geol. Soc. Am. Bull.*, 89:591–604.
- Le Maitre, R.W., Bateman, P., Dudek, A., Keller, J., Lameyre Le Bas, M.J., Sabine, P.A., Schmid, R., Sorensen, H., Streckeisen, A., Woolley, A.R., and Zanettin, B., 1989. *Classification of Igneous Rocks and Glossary of Terms*. Oxford (Blackwell).
- Mahood, G.A., and Hildreth, W., 1986. Geology of the peralkaline volcano at Pantelleria, Strait of Sicily. *Bull. Volcanol.*, 48:143–172.
- McCoy, F.W., 1981. Areal distribution, redeposition and mixing of tephra within deep-sea sediments of the eastern Mediterranean Sea. In Self, S., and Sparks, R.S.J. (Eds.), *Tephra Studies*. NATO Adv. Study Inst. Ser., 245:254.
- McCoy, F.W., and Cornell, W., 1990. Volcanoclastic sediments in the Tyrrhenian Basin. In Kastens, K.A., Mascle, J., et al., *Proc. ODP, Sci. Results*, 107: College Station, TX (Ocean Drilling Program), 291–305.
- Müller, C., 1990. Nannoplankton biostratigraphy and paleoenvironmental interpretations from the Tyrrhenian Sea, ODP Leg 107 (Western Mediterranean). In Kastens, K.A., Mascle, J., et al., *Proc. ODP Sci. Results*, 107: College station, TX (Ocean Drilling Program), 495–512.
- Nielsen, C.H., and Sigurdsson, H., 1981. Quantitative methods for electron microprobe analysis of sodium in natural and synthetic glasses. *Am. Mineral.*, 66:547–552.
- Paterne, M., 1985. Reconstruction de l'activité explosive des volcans de l'Italie du Sud par tephrochronologie marine [These Dr. Sci.]. Univ. Paris-Sud.
- Paterne, M., and Guichard, F., 1993. Triggering of volcanic pulses in the Campanian area, South Italy, by periodic deep magma influx. *J. Geophys. Res.*, 98:1861–1873.
- Paterne, M., Guichard, F., and Labeyrie, J., 1988. Explosive activity of the south Italian volcanoes during the past 80,000 years as determined by marine tephrochronologie. *J. Volcanol. Geotherm. Res.*, 34:153–172.
- Paterne, M., Guichard, F., Labeyrie, J., Gillot, P.Y., and Duplessy, J.C., 1986. Tyrrhenian Sea tephrochronology of the oxygen isotope record for the past 60,000 years. *Mar. Geol.*, 72:259–285.

- Paterne, M., Labeyrie, J., Guichard, F., Mazaud, A., and Maitre, F., 1990. Fluctuations of the Campanian explosive volcanic activity (South Italy) during the past 190,000 years, as determined by marine tephrachronology. *Earth Planet. Sci. Lett.*, 98:166–174.
- Rickwood, P.C., 1989. Boundary lines within petrological diagrams which use oxides of major and minor elements. *Lithos*, 22:247–263.
- Rio, D., Sprovieri, R., Thunell, R., Vergnaud Grazzini, C., and Glaçon, G., 1990. Pliocene–Pleistocene paleoenvironmental history of the western Mediterranean: synthesis of ODP Site 653 results. In Kastens, K.A., Masclé, J., et al., *Proc. ODP, Sci. Results*, 107: College Station, TX (Ocean Drilling Program), 695–704.
- Savelli, C., 1987. K/Ar ages and chemical data of volcanism in the western Pontine Islands (Tyrrenian Sea). *Boll. Soc. Geol. Ital.*, 106:537–546.
- , 1988. Late Oligocene to Recent episodes of magmatism in and around the Tyrrhenian Sea: implications for the processes of opening in a young inter-arc basin of intra-orogenic (Mediterranean) type. *Tectonophysics*, 146:163–181.
- Sartori, R., Masclé, G., and du Chaffaut, S.A., 1987. A review of Circum-Tyrrhenian regional geology. In Kastens, K.A., Masclé, J., Auoux, C., et al., *Proc. ODP, Init. Repts.*, 107: College Station, TX (Ocean Drilling Program), 37–64.
- Shipboard Scientific Party, 1996. Site 974. In Comas, M.C., Zahn, R., Klaus, A., et al., *Proc. ODP, Init. Repts.*, 161: College Station, TX (Ocean Drilling Program), 55–111.
- York, D., 1969. Least-squares fitting of a straight line with correlated errors. *Earth Planet. Sci. Lett.*, 5:320–324.

Date of initial receipt: 12 May 1997

Date of acceptance: 9 January 1998

Ms 161SR-265